DOI: 10.26599/FSHW.2025.9250709

Contents lists available at SciOpen

Food Science and Human Wellness

journal homepage: https://www.sciopen.com/journal/2097-0765

China Food Publishing Co.

High-phytosterol rapeseed oil prevents atherosclerosis by regulating liver lipid metabolism and intestine microbiota in ApoE$^{-/-}$ mice

Yaxi Xu[a,1], Mengxue Fang[a,1], Zhili Jin[b,d,1], Ze Chen[b,d], Tong Zhang[b,d], Li Yu[a], Fei Ma[a], Zhibing Lu[b,d,g], Hairong Wang[b,d,g,*], Liangxiao Zhang[a,c,e,f,*], Peiwu Li[a,c,h,*]

[a] *Key Laboratory of Biology and Genetic Improvement of Oil Crops, Ministry of Agriculture and Rural Affairs; Laboratory of Risk Assessment for Oilseed Products (Wuhan), Ministry of Agriculture and Rural Affairs; Quality Inspection and Test Center for Oilseed Products, Ministry of Agriculture and Rural Affairs; Oil Crops Research Institute, Chinese Academy of Agricultural Sciences, Wuhan, 430062, China*

[b] *Department of Cardiology, Zhongnan Hospital of Wuhan University, Wuhan 430071, China;*

[c] *Hubei Hongshan Laboratory, Wuhan, 430070, China*

[d] *Institute of Myocardial Injury and Repair, Wuhan University, Wuhan 430071, China*

[e] *College of Food Science and Engineering, Nanjing University of Finance and Economics/ Collaborative Innovation Center for Modern Grain Circulation and Safety, Nanjing, 210023, China*

[f] *Zhongyuan Research Center, Chinese Academy of Agricultural Sciences, Xinxiang, 453500, China*

[g] *Cardiovascular Institute, Zhongnan Hospital of Wuhan University, Wuhan, China*

[h] *Xianghu Laboratory, Hangzhou, 311231, China*

ABSTRACT: Atherosclerosis (AS) is a worldwide disease caused by disorders of lipid metabolism, and lipid deposition in artery walls. The study aims to evaluate the effect of high-phytosterol rapeseed oil (HPRO) on the prevention of AS and elucidate the mechanism involved by exploring the composition of liver lipids, lipid synthesis, and metagenomes. The results show that HPRO reduces dyslipidemia and lipid accumulation in mice, and prevents AS lesions. By liver lipidomics analysis, we found that HPRO prevents AS by regulating the pathways of lipid and atherosclerosis, and glycerolipid metabolism. HPRO was shown to down-regulate the protein expression level of liver lipid synthesis markers sterol regulatory element-binding protein 1 and fatty acid synthase via AMP-activated protein kinase, and this is superior to that of β-sitosterol. Through metagenomic analysis, we found that HPRO increased the levels of beneficial bacteria *Bacillota* and *Muribaculaceae* while decreasing the levels of harmful bacteria *Enterobacterales* and *Pseudomonadota*. Interestingly, correlation analysis of liver lipids, intestinal flora, and AS indicators found significant correlations among them.

Keywords: High-phytosterol rapeseed oil; Liver lipid metabolism; Gut microbiota; Atherosclerosis;

1. Introduction

Atherosclerosis (AS) is the most common type of cardiovascular disease, primarily characterized by the buildup of lipids and inflammatory responses within large arteries. This condition can ultimately result in

[1] These authors contributed equally to this work.
***Corresponding author**
peiwuli@oilcrop.cn (P. Li); zhanglx@caas.cn (L. Zhang)
zn000008@whu.edu.cn (H. Wang)

Received 29 January 2025
Received in revised from 27 February 2025
Accepted 10 June 2025

serious health issues, including myocardial infarction and stroke. The high occurrence of unhealthy dietary habits might play a part in this progression, with diet being crucial in the prevention of AS [1-3].

Phytosterols play a crucial role as micronutrients within the human diet, possessing the capability to lower serum cholesterol levels and diminish the risk of cardiovascular and cerebrovascular diseases. An abnormal cholesterol level or a dysfunction in lipid metabolism specifically acts as an autonomous risk determinant for AS [4]. The cholesterol levels and homeostasis in the body, are affected by how this is made in the liver and how it is absorbed in the intestine [5]. The small intestine is essential for both cholesterol synthesis and lipoprotein metabolism. Furthermore, it is responsible for absorbing cholesterol derived from the diet as well as from the body's own biliary secretion [6]. Research has shown that phytosterols can hinder the uptake of cholesterol, from both food and endogenous (biliary) sources within intestinal cells. This blocking leads to a decrease in total serum cholesterol (TC) and low-density lipoprotein cholesterol (LDL-C) levels [7]. Additionally, phytosterol supplementation may modify the liver fatty acid content, significantly reducing saturated fatty acids and greatly increasing the levels of both monounsaturated and polyunsaturated fatty acids in the liver [8, 9].

The intestine microbiota significantly influences the onset, prevention, and management of AS [10-12]. Serving as a crucial regulator of the host's metabolism, the intestine bacteria display a composition and function that are adaptable and affected by dietary influences, particularly the amount and variety of lipids consumed. Moreover, phytosterols can boost the prevalence of beneficial microbes and metabolites that mitigate against AS [13]. The intestinal bacteria's effect on the host's fat metabolism might be enhanced by metabolites generated by these microbes, such as short-chain fatty acids, secondary bile acids, and trimethylamine, along with bacterial-derived pro-inflammatory agents, including lipopolysaccharide (LPS) [14]. In individuals with AS, alterations in the intestine bacteria occur, which are intimately linked to biomarkers of the disease, particularly plasma cholesterol levels [15-17]. Cholesterol is synthesized, broken down, and transformed in the liver [18]. Phytosterols can affect cholesterol transport in the blood by influencing both the formation and clearance of low-density lipoprotein (LDL) [19]. LDL serves a crucial function in transporting cholesterol synthesized in the body, while phytosterols can modify serum LDL levels [20, 21]. Therefore, regulating the composition of intestinal flora, and optimizing liver lipid and cholesterol metabolism are new strategies to prevent AS.

Nevertheless, currently, the consumption of phytosterols remains quite low in several countries. The primary sources of phytosterols are edible vegetable oils, with rapeseed oil being the most significant contributor, representing 22.9% of the overall phytosterol consumption from all types of foods [22], and intake of phytosterols with oil are more beneficial to play a role in lowering serum cholesterol [23]. There is growing evidence to support the use of nutrient-rich whole rapeseed oil to prevent AS and as an important component of a healthy diet [24]. Consequently, high-phytosterol rapeseed oil (HPRO) has great potential in interventions to reduce AS. Therefore, the objective of this study was to examine the impact of HPRO on intestinal microbiota structure and liver lipid metabolism in AS mice. The changes in serum TC, triglyceride (TG),

LDL-C, high-density lipoprotein cholesterol (HDL-C), and aortic plaque, reactive oxygen species (ROS), and CD45R AS parameters were studied. In addition, alterations in the lipid structure change by lipidomics analysis and intestine flora of mice were evaluated by metagenic sequencing analysis to elucidate the regulatory role of HPRO on the lipids and microbiota composition and function of atherosclerotic mice. Meanwhile, we also investigated the reducing effect of HPRO on lipid metabolism and the reducing effect of lipid synthesis markers SREBP-1 and fatty acid synthase (FASN) expression. This study should give a scientific foundation for the application of HPRO to the prevention of AS.

2. Materials and methods

2.1. Diets, animals, and experimental design

All animal experiments adhered to ARRIVE guidelines. Under permission number HLK-20230605-003, the experimental protocols were authorized by the Animal Ethics Committee and Wuhan Halic Biotechnology Co., Ltd. Mice deficient in apolipoprotein E ($ApoE^{-/-}$ mice) are a commonly used model of atherosclerosis, and their lesions are similar to those of humans [25]. 6-week-old C57BL/6J and ApoE knockout male mice (C57/BL6 background) were acquired from GemPharmatech Co., Ltd. (Nanjing, Jiangsu, China). Experimental design and operation follow the principle of reducing animal suffering. All mice were given adequate food and drinking water in a 12 h dark/light cycling environment. Three groups of mice were created and given three different diets provided by Beijing HFK Biotechnology Co., Ltd. (Beijing, China) icluding the control group fed by a standard diet (6 male C57BL/6J mice), the western diet (WD, Supplementary file Table S1) group (6 male $ApoE^{-/-}$ mice), HPRO group (6 male $ApoE^{-/-}$ mice) fed by WD containing HPRO instead of the corn oil and anhydrous milk fat component[26]. The experimental protocol was carried out over a period of 21 weeks.

2.2. Serum and tissue measurements and staining

Upon conclusion of the experiment, the mice underwent fasting, and 6 mice in each group were euthanized and quickly obtained blood specimens, and the aorta, adipose, and liver tissues were stained and preserved. Liver levels of superoxide dismutase (SOD), malondialdehyde (MDA), tumor necrosis factor-α (TNF-α), interleukin-6 (IL-6), alanine aminotransferase (ALT), and aspartate aminotransferase (AST) and blood lipid levels were quantified in accordance with the directives of commercial kits.

2.3. Histological examination

Mice tissues from the aorta and liver, which were stabilized with paraformaldehyde, were placed, and sections were prepared for both ORO and H&E staining. The ORO dye dissolves readily and can penetrate cell membranes to attach to lipid droplets found within cells. This dye's specific affinity for lipids allows the regions containing them to be distinctly revealed in red under a light microscope, whereas other areas remain colorless or show different hues. During Hematoxylin-Eosin (H&E) staining, chromatin, and cytoplasmic nucleic acids acquire a purple-blue tint, with the nucleus displaying a rich blue shade. The cytoplasmic

regions, along with the extracellular matrix, appear pink as a result of eosin staining, emphasizing the overall tissue architecture and the unique structural characteristics of the lesion.

2.4. CD45R levels in peripheral blood and aorta ROS level

The samples were subjected to centrifugation at 2, 000 r/min for a duration of 5 min and later mixed again in 1 ml of PBS. After washing, they were centrifuged once more, with the supernatant discarded. Two distinct groups were created: the unfilled standard group and the flow single standard group. In the case of the blank standard tube, 100 μL of PBS was incorporated, omitting any antibodies. Following this, an additional 2 mL of PBS was used for rinsing, which was thereafter subjected to additional centrifugation at 2, 000 r/min for 5 min at 4 ℃ to effectively eliminate the extra fluid. The cells were then reintroduced to suspension into 100 μL of PBS which was maintained in the dark at 4 ℃ until analysis. The analysis of the experimental results was carried out utilizing NovoExpress software.

The ROS level was detected by flow cytometry: DCFH-DA was diluted at a ratio of 1:1000, and cells were collected. After incubation, cells were washed with serum-free cell medium, and then cells were collected and re-suspended with PBS for on-machine detection. The analysis was performed using NovoCyte analysis software.

2.5. Transmission electron microscope

A petri dish equipped with an electron microscope fixation solution was prepared in advance before sampling, and the small tissue blocks were put into the petri dish immediately for fixation after being removed in vitro. This was followed by post-fixation and room-temperature dehydration. The permeable package was kept in the oven overnight. After 48 h of polymerization, it was positioned under a light microscope. After the copper mesh was dyed, the slices were put into a box kept dry at room temperature, and observed and analyzed after 12 h.

2.6. Liver lipidomics analysis

In this study, the preparation standard of mouse liver samples was 100 mg/sample, and the samples were stored at -80 ℃ after being quick-frozen in liquid nitrogen and transported in dry ice. Targeted detection of lipid molecules, Q-TRAP instrument, and MRM gold quantitative mode, Rt+Q1/Q3 multiple ions accurate qualitative substances, analysis in the database. The identified metabolites were annotated in the KEGG database and fed back to the KEGG Pathway database.

2.7. Small intestinal contents metagenomic sequencing

Samples were removed from the small intestine of the mice with a sample size of about 1 g. The entire small intestine was excised with a clean blade, the materials were cut on the sterile operating table, and the contents were excavated with a clean knife and then immediately placed on ice for subpacking and marking. The samples were subpacked to avoid repeated freezing and thawing. The steps used were: sample DNA extraction and detection, library construction detection, sequencing quality control, and analysis. When sample contamination is suspected, it is essential to compare with the host database to eliminate reads that

might be derived from the host. Where this is the case the parameters have to be changed. Following this, metagenome assembly, gene prediction, abundance assessments, and species annotation were performed.

2.8. In vitro simulated digestion

The digestion of HPRO was conducted in vitro in accordance with the standardized INFOGEST protocol [27]. Simulated saliva, gastric, and intestinal fluids were prepared. Once the intestinal stage is over, digestion stops. The specimen was rapidly frozen using liquid nitrogen maintained at -80 ℃ for subsequent analytical purposes.

2.9. Caco-2/HepG2 cultures and identification of intracellular lipid reduction in a Caco-2/HepG2 coculture model

Caco-2 cells were inoculated into 12-well plates and incubated at 37 ℃ and 5% CO_2 for 24 h. The culture medium needs to be renewed every other day to ensure the cells mature for at least 21 days. The medium was replaced in a timely manner to ensure cell maturation for at least 21 days, and a membrane with a transepithelial resistance (TEER) value greater than 400 Ω cm^2 was considered a successful model [28]. D-HPRO was introduced at a dilution of 1:8 to the apical (AP) side [29], and the β-sitosterol levels in the D-HPRO group were kept at the same as those in the 100 μmol/L β-sitosterol intervention group. On the 19th day of culture, HepG2 cells were inoculated on the basolateral (BL) side to establish a co-culture model. After an incubation period of 24 h, the high-fat treatment was introduced along with sodium oleate (NAOL) solution. Finally, samples were extracted and tested from the well. The lipid-lowering effect of the extract was tested using a test kit, and the concentration of each well was quantified, in line with the manufacturer's guidelines. The lipid-lowering properties of D-HPRO and β-sitosterol were evaluated in an experimental setting.

2.10. Western blot analysis

The separated samples were placed onto PVDF membranes (Millipore Corp., Massachusetts, United States). Blocking of the PVDF membrane was carried out for 1 h at ambient temperature utilizing a blocking solution. Following this, immunoblots were conducted utilizing primary antibodies specific to the target protein along with an internal control protein. To facilitate detection, a secondary antibody conjugated to horseradish peroxidase was introduced to the blot. Ultimately, the gray values associated with the target protein blots, adjusted for β-actin, were evaluated using the Tanon Gis software (Tanon, Shanghai China).

2.11. Molecular docking

The structures of the compounds were sourced from the PubChem database, while the protein's three-dimensional configurations were retrieved from the PDB database. Docking site pocket detection and blind docking were carried out successively, and the ligand molecules were hydrogenated and partially charged to generate the initial 3D conformation, the addition of side chain atoms and hydrogen atoms missing from the receptor protein, and the removal of crystal water. The methods utilized were referenced from earlier studies [30, 31].

2.12. Statistical Analysis

Results are presented as mean ± standard error of the mean (SEM). The experiments were assessed through ANOVA for a comparative analysis of multiple groups and Student's t-test for a comparative analysis of two groups, with a significance level established at $P < 0.05$. All analyses were performed using GraphPad Prism version 9 software (GraphPad Software, San Diego, USA) and the Graphical abstract was created with BioRender.com.

3. Results

3.1. Body weight and adipose tissue morphology in mice

The buildup of both visceral and subcutaneous fat increases the risk of AS [32]. Fat dysfunction caused by obesity is the main factor associated with AS [33]. In Table 1, no substantial variation in food consumption was seen across the three groups. When ApoE$^{-/-}$ mice were provided with a WD, their body mass increased by (10.33 ± 0.53) g, which was significantly elevated compared to the Control group. Fig. 1A shows that, compared with WD mice, the HPRO intervention significantly reduced body weight. Research indicates that an elevation in fatty acid release from white adipose tissue (WAT), along with a reduction in lipid oxidation from brown adipose tissue (BAT), results in hyperlipidemia, ultimately contributing to the onset of AS [34]. In addition to its effect on body weight, HPRO also has an apparent antiobesity impact on adipose tissue. Fig. 1B, C, D and E show that WAT, including inguinal white adipose tissue (iWAT), retroperitoneal white adipose tissue (rWAT), and epididymal white adipose tissue (eWAT), appeared more prominent in WD mice than in the control group, whereas HPRO feeding substantially diminished fat accumulation. There were no discernible differences in interscapular brown adipose tissue (iBAT) among the three groups. As shown in Fig. 1F and 1G, the dimensions of lipid droplets and the area of adipocytes in the epididymal tissue of the WD group were substantially greater than those in the control group. Feeding HPRO prevented fat building up in fatty tissue. The white adipose tissue cells in the WD group were considerably larger than those in the control group, and cell membrane rupture could be seen. After HPRO treatment, the surface area of white adipocytes was smaller, and the cell membrane was evident.

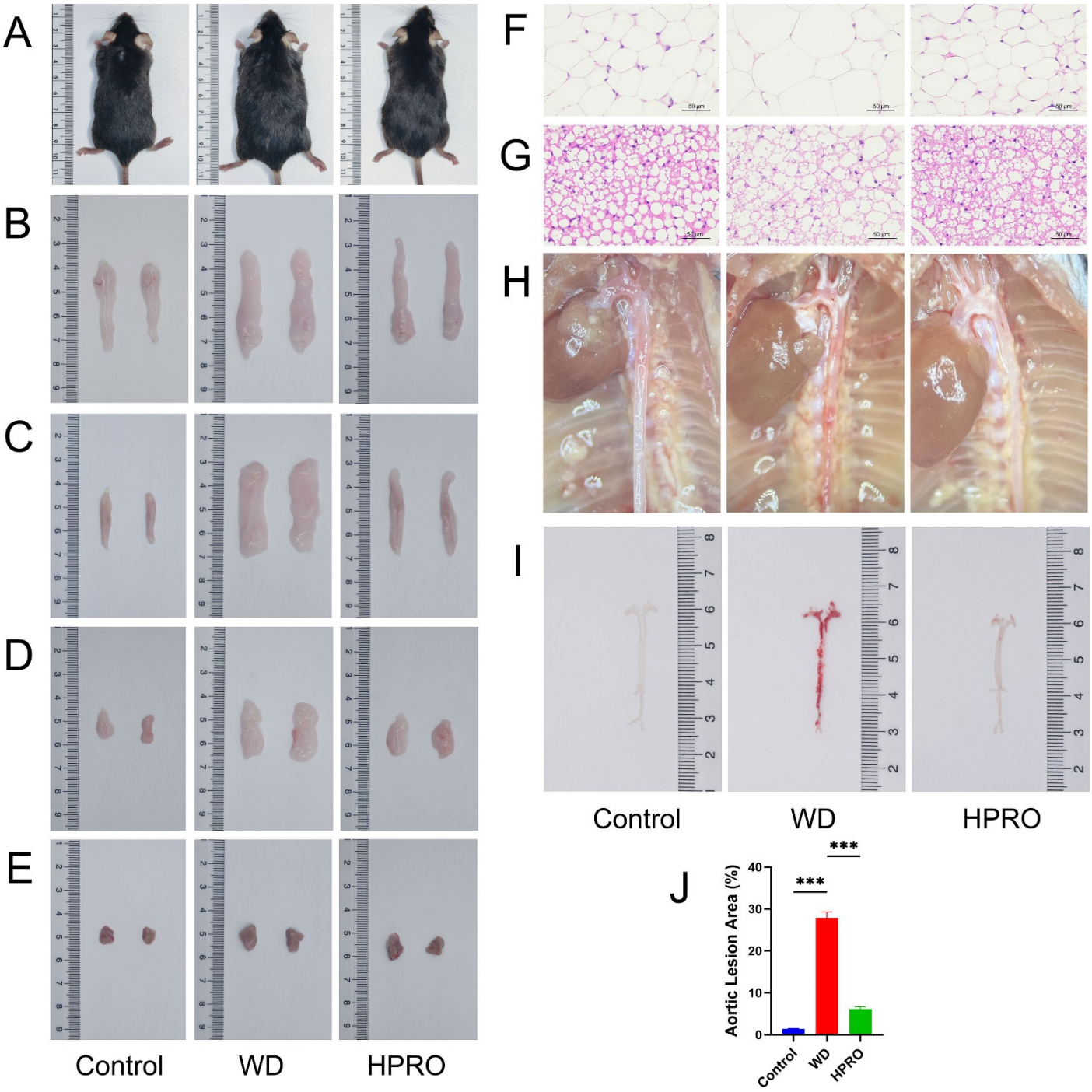

Fig. 1. Effect of HPRO on body weight and fat appearances in mice. (A) representative photographs of each group of mice at the end of 21 weeks. (B) epididymal white adipose tissue, eWAT. (C) Inguinal White Adipose Tissue, iWAT. (D) retroperitoneal white adipose tissue, rWAT. (E) Interscapular activated brown adipose tissue, iBAT. Effect of HPRO structured lipids on adipose tissue morphology in WD mice. (F) White adipose tissue, WAT. (G) Brown adipose tissue, BAT. (H) Representative in situ images of atherosclerotic plaque in the aortic arch of mice. (I) ORO staining of the aorta in mice. Lipid deposition was quantified using ImageJ. (J) Quantitative analyses of aortic lesion (%). The data are presented as the mean ± SEM, n = 6. *** $P < 0.001$.

Table 1. Effect of HPRO on fundamental metrics.

Items	Control	WD	HPRO
Initial body weight (g)	22.10 ± 0.28	22.20± 0.22	22.20 ± 0.26
Final body weight (g)	29.18 ± 0.34***	32.53 ± 0.41	30.75 ± 0.19**
Body weight gain (g)	7.08 ± 0.36***	10.33 ± 0.53	8.55 ± 0.20**
Food intake (g/day)	3.53 ± 0.09	3.61 ± 0.08	3.53 ± 0.06
Liver index	4.81 ± 0.11***	5.77 ± 0.17	4.95 ± 0.11**
Liver SOD (U/mg prot)	140.61 ± 3.81***	95.20 ± 3.54	149.85 ± 6.00***

Liver MDA (nmol/mg prot)	1.00 ± 0.04***	2.13 ± 0.10	1.30 ± 0.03***
Liver TNF-α (pg/mg prot)	115.12 ± 6.77***	182.14 ± 9.66	129.34 ± 5.48***
Liver IL-6 (pg/mg prot)	21.00 ± 1.55***	51.03 ± 2.62	31.48 ± 2.59***
Liver ALT (U/g prot)	43.84 ± 2.14***	106.37 ± 4.40	53.94 ± 3.19***
Liver AST (U/g prot)	12.04 ± 0.91***	22.17 ± 1.09	14.07 ± 0.83***
TC (mmol/L)	15.37 ± 0.72***	27.08 ± 1.85	16.70 ± 1.72***
LDL-C (mmol/L)	2.45 ± 0.27***	10.53 ± 1.61	3.74 ± 1.38**
HDL-C (mmol/L)	2.54 ± 0.07**	1.91 ± 0.12	2.53 ± 0.17**
TG (mmol/L)	1.93 ± 0.13**	2.50 ± 0.15	1.41 ± 0.04***

Values are expressed as mean ± SEM, n = 6, independent experiments. ** $P < 0.01$, *** $P < 0.001$ compared with the WD group.

3.2. Effect of HPRO on AS physiological parameters in mice

3.2.1. Lipid profile

Dyslipidemia, characterized by LDL-C levels, can lead to atherosclerotic cardiovascular disease and serves as a significant marker for detection [35-37]. In Table 1, ApoE$^{-/-}$ mice showed elevated TC, TG, and LDL-C levels due to disordered cholesterol and lipid metabolism. HPRO treatment reduced serum TG, TC, and LDL-C levels, and HDL-C levels significantly increased.

3.2.2. Atherosclerotic lesions

Aortic plaque is an important indicator for the evaluation of AS. The in situ photography and ORO-stained whole aorta lesions showed that the aortic plaque was increased in the mice fed the WD and those given HPRO treatment showed lower levels (Fig. 1H and I). ORO fat staining makes the fat in the tissue red and is used to detect fat in the tissues. In Fig. 1I the intimal atherosclerotic lesions of the aorta were longitudinally sliced and subjected to staining with ORO. The findings indicate that the WD group exhibited significant lipid accumulation, which was extensively spread from the aortic arch to the bifurcation of the femoral artery. Conversely, the HPRO group exhibited significantly lower lipid plaque areas, showing only limited lipid accumulation in the aortic arch relative to the WD group. The control group exhibited virtually no lipid accumulation. The proportion of the lesion area to the aggregate area of the aorta was 1.40% for the control group and 6.12% for the HPRO group. This ratio in the HPRO group was considerably below that observed in the WD group, which was 27.90% (Fig. 1J).

H&E staining can stain all the components of the tissue making it suitable for comprehensive observation of the tissue structure. In Fig. 2A, In the control group, vascular tissue staining is uniform, each layer structure is clear, the inner membrane vascular endothelium (black arrow) structure is complete, the medium membrane smooth muscle cells (yellow arrow) shape and structure is normal, clear demarcation, the outer membrane (red arrow) collagen fiber content is rich, regular arrangement, no obvious inflammatory cell infiltration. In the WD group, vascular plaque formation, intima thickening, connective tissue hyperplasia (black arrow), accompanied by a small amount of foam cell infiltration (yellow arrow) can be seen in the vascular tissue. A small amount of vascular smooth muscle cell degeneration (red arrow), cell swelling, loose cytoplasm, and a small amount of lymphocyte infiltration (blue arrow) can be seen in the media and outer membranes. In the HPRO group, A small amount of endothelial cells can be seen shedding in blood vessels (brown arrow), and local red blood cells can be seen sticking to the wall (green arrow). The smooth muscle

cells in the medium membrane had normal morphology and structure, clear boundary, abundant collagen fibers in the outer membrane, regular arrangement, and no obvious inflammatory cell infiltration. H&E staining showed that the area of atherosclerotic lesions in the WD model group was more significant than in the control group. The HPRO substantially diminished the area of atherosclerotic plaques in mice aortae.

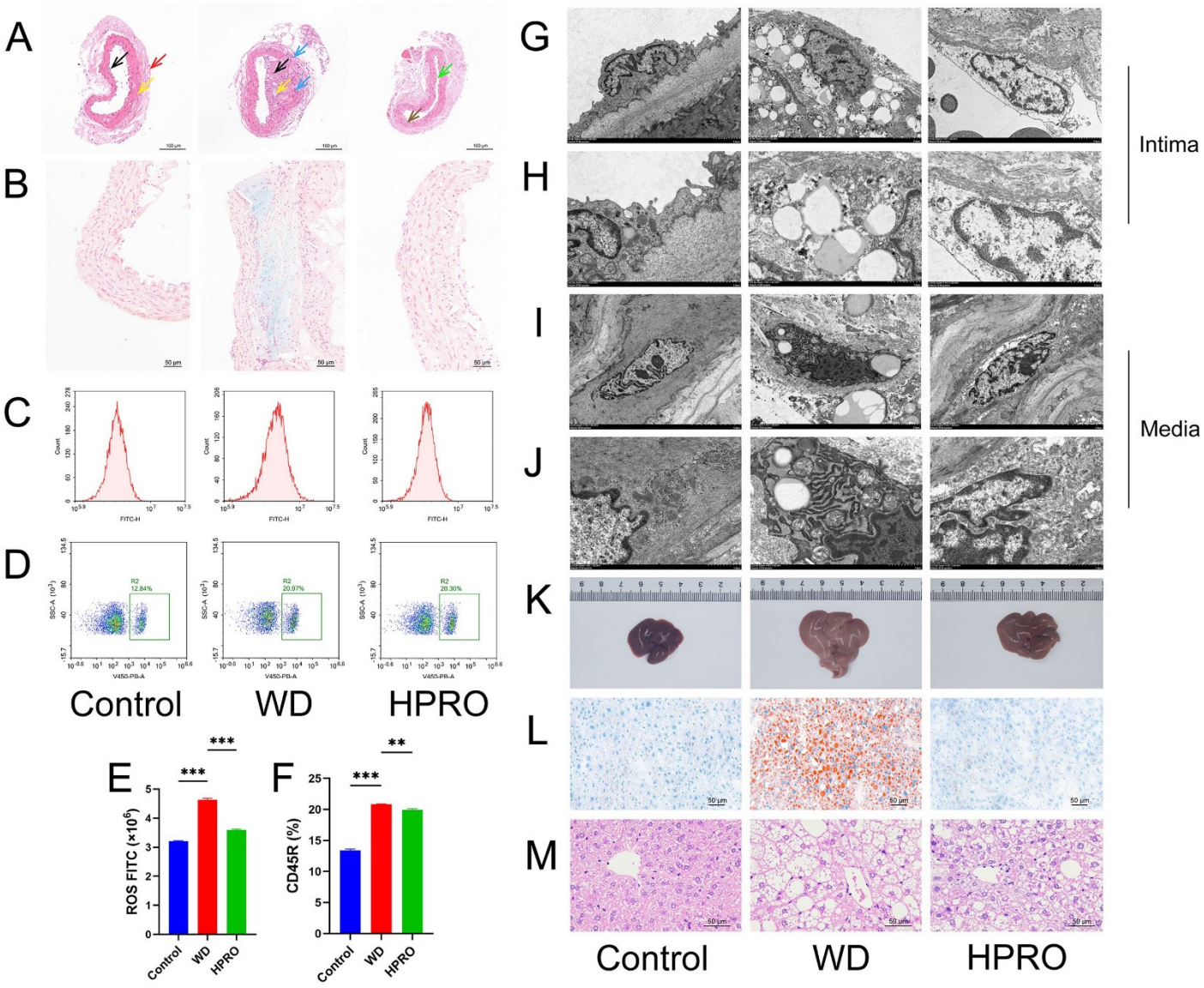

Fig. 2. Effect of HPRO on the formation of atherosclerotic lesions. (A) H&E staining of the aorta; magnification 400×. (B) β-Gal staining in the aorta. (C) ROS levels in the aorta by flow cytometry. (D) CD45R levels in the aorta by flow cytometry. (E, F) Quantitative analyses of ROS, CD45R. (G, H) Transmission Electron Microscope images of tunica intima. (I, J) Transmission Electron Microscope images of tunica media. (K, L, M) Control, WD, and HPRO, representative photographs of mice liver, ORO staining, and H&E staining. The data are presented as the mean ± SEM, n = 6. ** $P < 0.01$; *** $P < 0.001$.

Aging is one of the most significant risk factors for AS [38]. The process of aging may directly influence the vasculature in a proatherogenic manner [39, 40]. β-Gal serves as a biological indicator that signifies cellular senescence [41]. In Fig. 2B, in comparison to the control group, the positive area of β-Gal in the WD group increased significantly. At the same time, it decreased substantially in the HPRO group β-Gal positive region, slowing down the aging caused by WD.

3.2.3. Aorta oxidative eustress

Overproduction of reactive oxygen species (ROS) results in oxidative stress which makes a substantial contribution to the onset and advancement of AS [42]. Fig. 2C and E show that the WD group increased ROS to 4.63×10^6 compared with 3.21×10^6 in the control group. After HPRO treatment, the FITC fluorescence decreased to 3.60×10^6. CD45R is a cell surface protein, research has demonstrated that the expression level of CD45R is intimately connected to the occurrence and development of AS. Alterations in the expression levels and composition of the CD45R molecule may contribute to the development of AS and various other medical conditions [43-45]. The levels of CD45R in the WD group were markedly elevated in comparison to the control group, while those in the HPRO group were substantially lower than those in the WD group (Fig. 2D and F). The above results show that HPRO has a mitigating effect.

3.2.4. Aortic micromorphology

AS in humans is strongly linked to the intimal and medial aortic layers, with lesions categorized and detailed as follows: early lesions, fatty spots and streaks, intermediate lesions, fibrous fatty plaques, and complex lesions [46, 47]. TEM can visualize the internal morphology and ultrastructure of the aorta, so this was used to analyze the lesions of the intima and media.

In the tunica intima results of TEM, some differences in the intima were shown between the three groups (Fig. 2G and H). The images of the WD group showed that the vascular intima was severely damaged, and most of the endothelial cells had fallen off and disintegrated; the atherosclerotic plaques were large, and a substantial number of foam cells had gathered. The images of the HPRO group showed moderate intimal injury, edema and rounding of endothelial cells, uneven structure of the internal elastic membrane, and local breakage. In the control group, the overall structure of the vascular intima was relatively normal, the endothelial cells were flat and long fusiform, and the internal elastic membrane structure was acceptable.

Results of TEM of the tunica media showed some differences between the three groups (Fig. 2I and J). Among them, the images of the WD group showed that the tunica media was seriously damaged, a large area of atherosclerotic plaques could be seen, and many lipid droplets and cholesterol crystals were distributed inside and outside the cells. The number of smooth muscle cells was significantly reduced, with large areas of pyknosis and apoptosis. The images of the HPRO group showed mild damage to the vascular structures of the tunica media, little edema of smooth muscle cells with an irregular shape, significantly enlarged intercellular space, increased interstitial tissue, and swollen organelles. The images of the control group exhibited that the structure of the tunica media was typical, the smooth muscle cells were evenly distributed between the basal lamina in a contracting state, the structure was fair, the thickness of the basal lamina was uniform, and the fiber structure was dense. From the above results, it can be seen that HPRO reduced the lesion damage in the intima and media.

3.3. Liver lesion and lipid composition

3.3.1. Tissue and cytokines status

The histopathological alterations in the liver across different groups were evaluated using a variety of methods (Fig. 2K, L, and M). The macroscopic examination indicated that the livers of rats fed a WD

exhibited a lighter coloration compared to those in the control group due to fat accumulation. Additionally, ORO staining demonstrated significant lipid accumulation in the livers of the WD group. H&E staining illustrated necrosis of liver cells and the presence of inflammatory cell infiltration in the WD group. In contrast, the administration of HPRO lessened these detrimental effects.

AS is associated with oxidative stress, inflammation, lipid peroxidation, and increased activity of liver enzymes, and this is observed during all stages of AS progression [48-50]. In comparison to the WD group (Table 1), the HPRO group demonstrated significant improvement in liver index and liver SOD, MDA, TNF-α, IL-6, ALT, and AST, the WD group had significantly higher liver weights than the other groups, which can be attributed to their long time consumption of WD, resulting increased liver fat accumulation. The liver index decreased from 5.77 in the model group to 4.95 in the HPRO group, congruent with previous research [51]. These data indicated that HPRO administration improved the serum lipid profiles, inhibited Oxidative Stress, and reduced proinflammatory factors, and liver index in the liver. To conclude, our results demonstrated that HPRO treatment significantly optimized blood fat and AS-related physiological parameters in ApoE$^{-/-}$ mice fed with WD.

3.3.2. The count of lipid types within lipid categories

This study classifies results according to lipid differences these are shown in Fig. 3A. The mice liver lipidomics analysis showed 1454 lipids that were divided into 45 groups, which were classified as follows: bile acid (BA), cholesterol ester (CE), ceramide (Cer-AP), cholesterol (Cho), coenzyme Q (CoQ), diglyceride (DG), Diglycerol (ether bond) (DG-O), oxidized Lipid (Eicosanoid), free fatty acid (FFA), triglyceride (TG), Triglycerides (ether bond) (TG-O) et al. In the present study, TG had the highest difference, followed by PE.

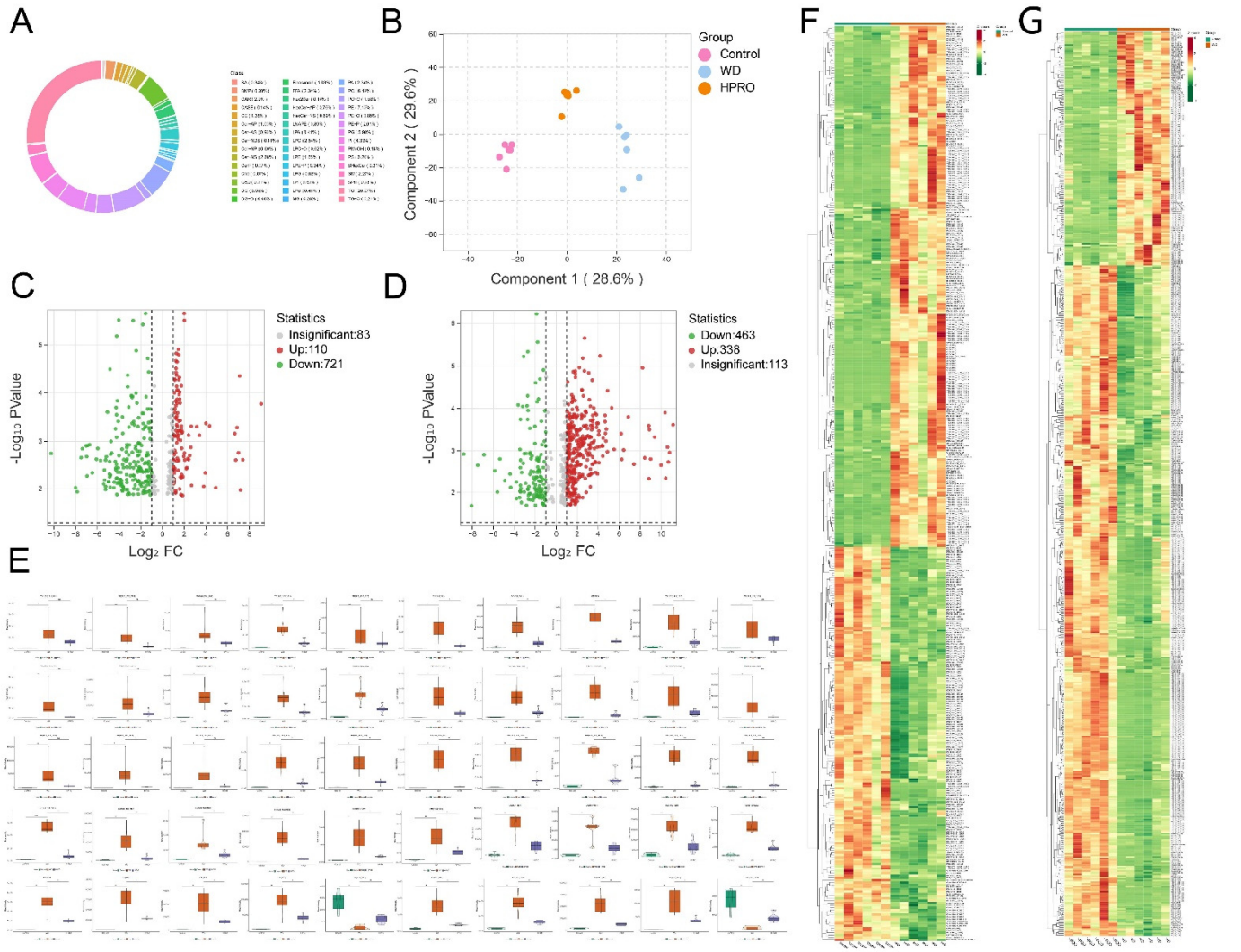

Fig. 3. Lipidomics analysis of mice liver samples. (A) The lipid subclasses constitute a ring diagram. Each color represents a lipid subclass, and the color block area indicates the proportion of that category. (B) OPLS-DA score plot of liver lipid profiles of all samples. (C) Volcano plots of control vs. WD. (D) Volcano plots of WD vs. HPRO. (E) Violin plot of corresponding group differential lipids in the liver. (F) Different lipids in control vs. WD. (G) Different lipids in WD vs. HPRO. * $P < 0.05$; ** $P < 0.01$; *** $P < 0.001$; **** $P < 0.0001$.

3.3.3. Difference analysis of liver lipids

As demonstrated in Fig. 3B, the samples obtained from both the control and WD groups were clearly differentiated and situated at a significant distance from one another, indicating a low degree of similarity. This finding further suggests that the WD resulted in significant changes to the liver lipid profile in the mice. Correspondingly, the specimens from the WD and HPRO groups were also noticeably disjoined and located at a distance, reflecting minimal similarity between these two sets and underscoring the considerable alterations in the AS condition of the mice after HPRO treatment.

A volcano plot was utilized to represent the comprehensive distribution of differentially expressed lipids. Lipid categories were established based on Log2 (|Fold Change|, |FC|) values greater than 1 (adjusted *p* values less than 0.05). An increase in Log2 (Fold Change, FC) indicates the up-regulation of certain lipids, while a decrease reflects their down-regulation. As shown in Fig. 3C and D, the WD group displayed 831 unique lipids in comparison to the control group. Conversely, the HPRO group revealed 801 distinct lipids when compared with the WD group. We then performed an analysis of the differential lipids among the groups.

In Fig. 3E, in contrast to the WD group, PE (17:0_22:5), PG (18:1_16:1), PC (12:0_18:1), PC (14:1_16:1), CE (16:0), CE (17:1), CE (20:2), CE (20:3), Cer (d16:1/23:0), DG (14:0_18:1), DG (15:0_18:1), DG (17:1_18:1), SM (d18:0/14:0), SM (d18:1/12:0), TG (15:0 _16:0 _18:0) et al were markedly elevated compared to the control group ($P < 0.01$), while HPRO intervention could significantly reduce the above lipid concentrations. In comparison to the control group, the contents of PE (22:2_18:0) and PA (20:2_22:5) in the WD group were significantly decreased ($P < 0.01$), and those in the HPRO group were significantly increased ($P < 0.01$). Therefore, HPRO regulates liver fatty acid composition, these lipids could serve as potential indicators for HPRO regulation of lipid metabolism in atherosclerotic mice.

3.3.4. Important lipid species in the liver

The heat map shown in Fig. 3F reveals that the control group displayed 400 different lipids when compared with the WD group. The lipids that were downregulated were primarily found in TGs, SMs, and CEs, whereas the upregulated lipids were mostly situated in PCs, PEs, and Carnitines. For the HPRO group, an aggregate of 581 different kinds of lipids was seen in comparison to the WD group (Fig. 3G), with the majority of upregulated lipids located in TGs and PEs. In contrast, the downregulated lipids were predominantly found in TGs, DGrs, and PEs. These results showed that the HPRO intervention substantially diminished disturbances in liver lipid metabolism by adjusting the levels of TGs and PEs. Additionally, we investigated the key and significant differential lipid species to identify specific lipid biomarkers associated with WD and HPRO.

3.3.5. Pathways in liver lipidomics

To examine the effect of HPRO on the metabolic pathways associated with differential lipids in the liver during the course of mitigating AS in mice, an enrichment analysis was conducted utilizing the metabolic routes of distinct lipid species from the KEGG database and these were categorized based on the types of KEGG pathways. Fig. 4A displays the comparative results for the control group, WD group, and HPRO group. HPRO influences lipid metabolism and AS, as well as glycerolipid metabolism. The KEGG classification of the differential metabolites is presented in Fig. 4B. Substantial alterations were observed in the degrees of organismal systems, metabolism, and human diseases. It has been hypothesized that HPRO may reduce AS by modulating metabolic pathways that alter lipid composition in the liver.

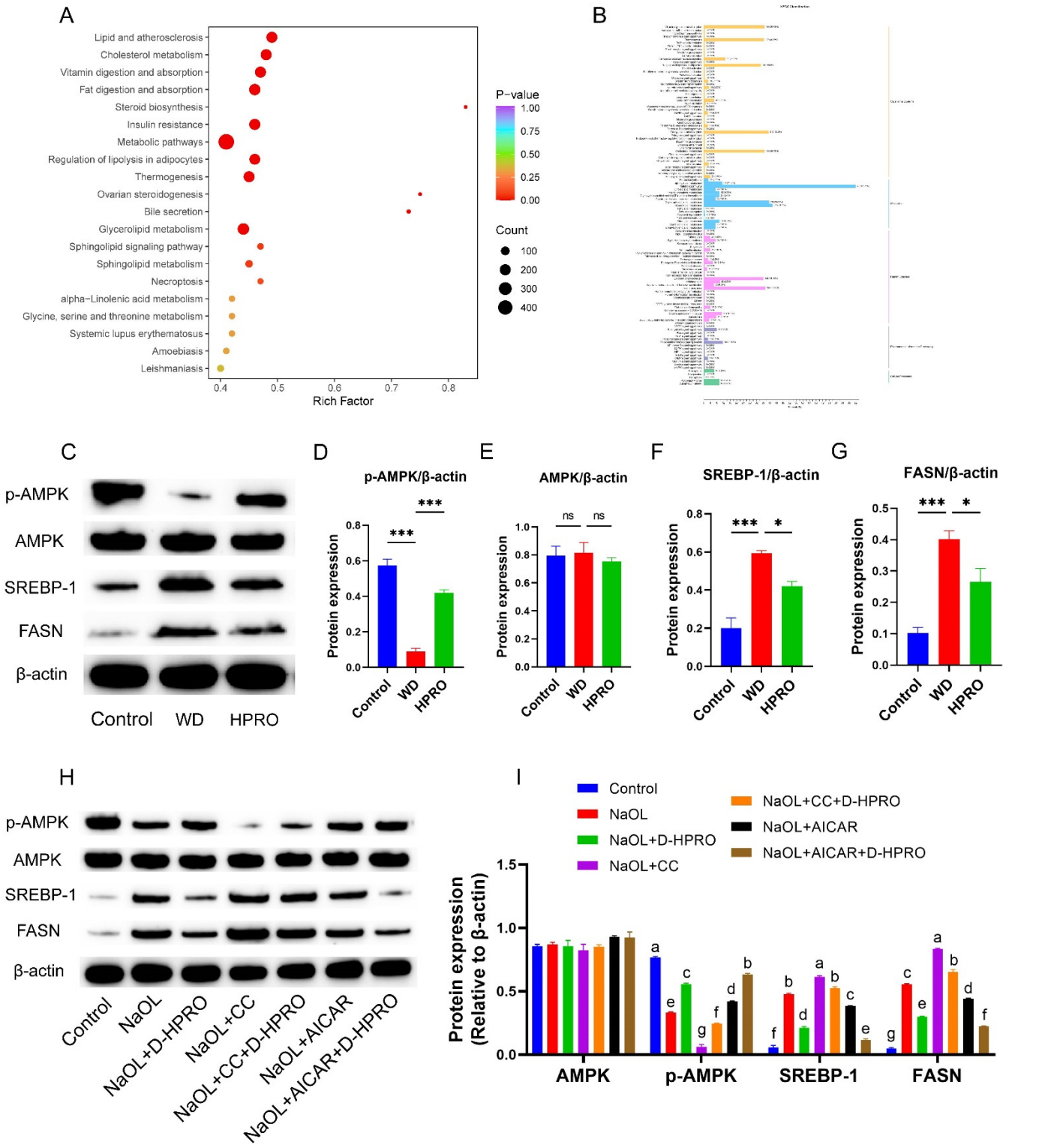

Fig. 4. (A) KEGG Enrichment. Lipid metabolism pathway analysis based on KEGG enrichment map for significantly different lipid species in control vs. WD vs. HPRO. In the metabolic pathway, the *p*-value was the significance of the metabolic pathway, and the significance-enriched path was selected for bubble mapping. The ordinate was the name of the metabolic pathway, and the abscissa was the Rich factor. The more significant the Rich Factor was, the greater the enrichment would be. The color from green to red indicated that the *p*-value decreased, and the lower *p*-value represents the more significant degree of enrichment. A larger dot suggests more metabolites were enriched on this pathway. (B) KEGG classification of differential lipids. Effect of HPRO on liver tissue pathology. (C, D, E, F, G) Protein expression of AMPK, p-AMPK, SREBP-1, and FASN in mice, n=3. (H-I) Protein expression of AMPK, p-AMPK, SREBP-1, and FASN in HepG2 cells, n=3. Diverse letters denoted a statistically significant difference ($P < 0.05$) among groups. * $P < 0.05$, *** $P < 0.001$.

3.3.6. Lipid synthesis at cellular and mice levels

FASN, crucial for the synthesis of fatty acids, represents a significant target of SREBP-1. As illustrated in Fig. 4C, D, E, F, and G, the findings indicated that the WD group had a notably lower expression level of p-AMPK compared to the control group. Conversely, the HPRO group exhibited a significantly elevated expression level of these proteins. Additionally, SREBP-1 and FASN showed a marked increase in their expression levels within the WD group relative to the control group, while these proteins' levels were considerably reduced in the HPRO group. HPRO was found to enhance the protein expression of p-AMPK and decrease lipid accumulation.

In Fig. 4H and 4I, to further investigate the underlying mechanism through which HPRO mitigates NAOL-induced steatosis in HepG2 cells, p-AMPK levels were assessed using western blot assay. Consistent with the findings observed in the AS mice model, D-HPRO significantly restored AMPK activity, with an increase in AMPK phosphorylation; at the same time, to confirm whether D-HPRO acts through AMPK, groups of AMPK activator (AIACR) and AMPK inhibitor (CC) were set. This effect was amplified by AIACR but diminished when CC was applied. Consequently, D-HPRO effectively reduced NAOL-induced liver lipid metabolism disorder in the mice liver by promoting AMPK phosphorylation and elevating the expression levels of SREBP-1 and FASN. Meanwhile, previous research has shown that phytosterol ester of α-linolenic acid and phytosterol can reduce lipid accumulation and SREBP-1 and FASN protein expression in HepG2 cells induced by NAOL. Among them, the phytosterol ester of α-linolenic acid is achieved by activating AMPK [52]. This provides support for the above mechanism of HPRO.

As shown in Fig. 5A, increasing β-sitosterol concentration above 100 μmol/L reduced the activity of HepG2 cells to less than 90% of the control group, and the selected D-HPRO and below 100 μmol/L β-sitosterol concentration was non-toxic to Caco-2 cells. The results in Fig. 5B showed that β-sitosterol could inhibit the lipase activity of HepG2 cells in a dose-dependent way. When the concentration of β-sitosterol was 100 μmol/L, the stipulation that the content of β-sitosterol was identical in the D-HPRO group, the inhibition rates of D-HPRO and β-sitosterol on lipase were close to 34.84%, and 25.74% respectively, indicating that D-HPRO had a better effect on reducing lipase activity than β-sitosterol.

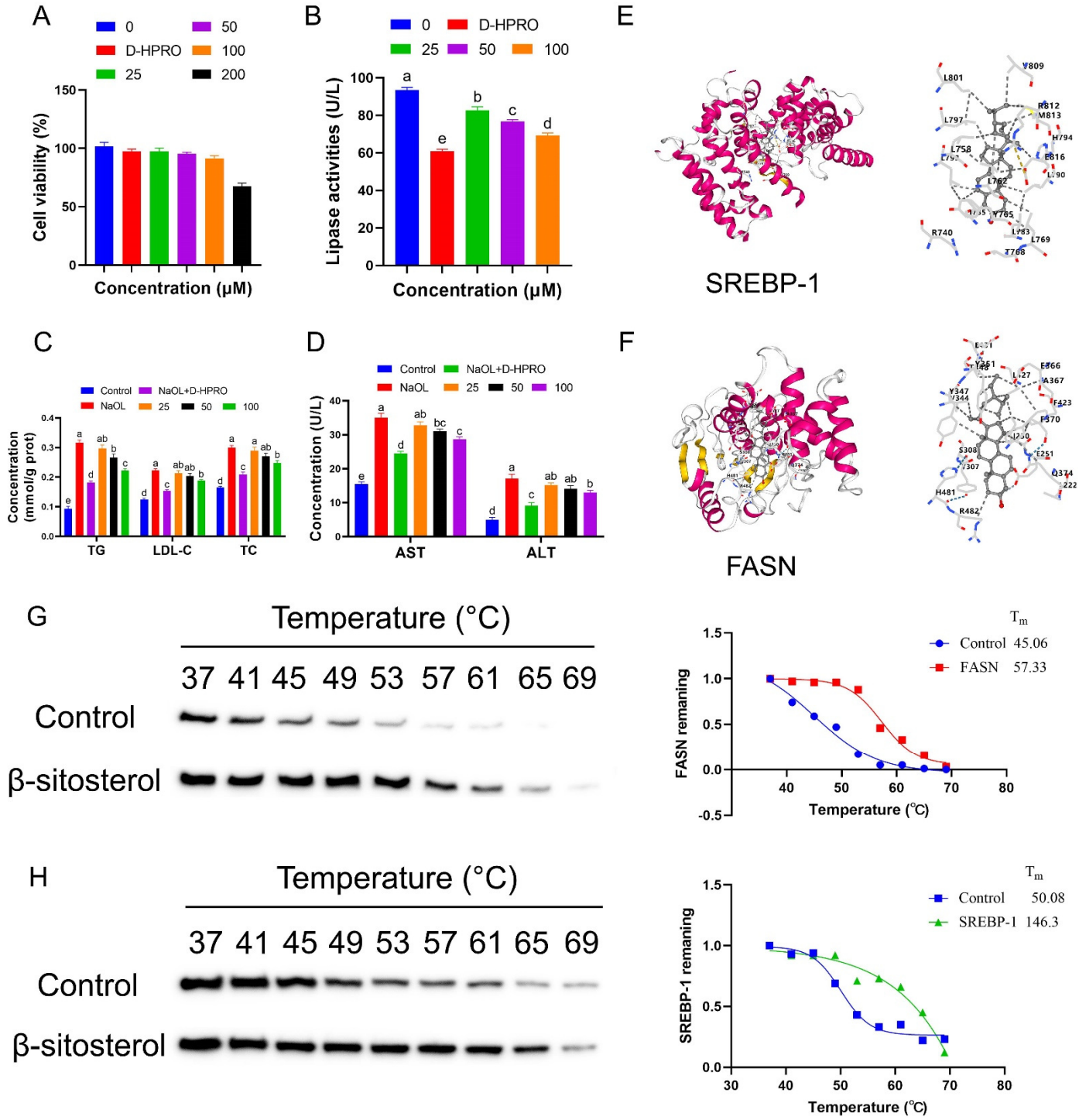

Fig. 5. Effect of polyphenol extract from D-HPRO and β-sitosterol on the (A) viability (B) inhibition of lipase of HepG2 cell lines. Lipid-lowering effects (C) TG, LDL-C, TC; (D) AST, ALT of D-HPRO and β-sitosterol on Caco-2/ HepG2 coculture models, n=6. Molecular docking results of β-sitosterol with four key targets. (E) β-sitosterol with SREBP-1, and (F) β-sitosterol with FASN. (G) The analysis curves represent the levels of HepG2 SREBP-1 protein in the control group and the β-sitosterol treatment group, (H) The analysis curves represent the levels of HepG2 FASN protein in the control group and the β-sitosterol treatment group, n=1. Diverse letters denoted a statistically significant difference ($P < 0.05$) among groups.

As shown in Fig. 5C and D, in order to understand the mechanism of lipid-lowering effects of the D-HPRO and β-sitosterol, the stipulation was made that the content of β-sitosterol was identical across the D-HPRO and 100 μmol/L β-sitosterol groups, and we measured the expression of relevant indicators of lipid metabolism at the level of HepG2 cells. The levels of TG, TC, LDL-C, AST, and ALT in HepG2 cells in the D-HPRO group and 100 μmol/L β-sitosterol group were significantly lower than those in the NAOL group,

and the results of D-HPRO were lower than those of 100 μmol/L β-sitosterol. Literature indicates that rapeseed oil possesses a substantial concentration of beneficial active compounds, including linoleic acid, α-linolenic acid, vitamin E, and carotene, which may account for the aforementioned outcomes [53]. Taken together, these results suggest that the HPRO group's lipid metabolism in HepG2 cells is reduced by the regulation of TG, TC, LDL-C, AST, and ALT levels, phytosterols in HPRO play a role in reducing lipid production, and the reduction impact of D-HPRO was superior to that of β-sitosterol.

3.3.7. Molecular docking analysis

Molecular docking is a theoretical simulation approach utilized to forecast the interactions between drugs and receptors, emphasizing their binding modes and affinities. In this investigation, the liver lipogenic proteins SREBP-1 (5gpd) and FASN (7mhd) were selected for molecular docking evaluation with the principal compound β-sitosterol. According to the findings presented in Table 2, the results obtained from the molecular docking revealed that the proteins exhibited substantial binding energies, accompanied by molecular docking visualizations in Fig. 5E and F. A lower binding energy indicates a higher binding affinity, facilitating the ligand's attachment to the receptor. It has been reported that molecular docking analysis of Quercetin and farnesol with SREBP-1 and FASN proved to be helpful in explaining the protective mechanism of Quercetin and farnesol in dyslipidemia [54, 55], which is consistent with our findings. This data highlighted the influence of the binding site of β-sitosterol on the target protein, reinforcing the results from the western blot analyses performed in this study.

Table 2. Molecular docking results of 2 critical proteins with β-sitosterol.

Compounds	Vina Score	
	SREBP-1 (5gpd)	FASN (7mhd)
β-sitosterol	-9.8	-9.5

Cellular thermal shift assay (CETSA) is used to investigate the thermal stability of proteins during ligand binding. The binding of ligands to proteins enhances thermal stability, thus enabling the identification of drug-target interactions[56]. Compared with the control group, we detected higher levels of SREBP-1 and FASN proteins in the β-sitosterol treatment group. As illustrated in Fig. 5G and H, both of thermal solubility curves of FASN and SREBP-1 proteins shifed signifcantly to the right after adding β-sitosterol, indicating that β-sitosterol enhanced the thermal stability of FASN and SREBP-1 proteins. The above results confirmed the specific binding between β-sitosterol and SREBP-1, FASN in molecular docking analysis .

3.4. Metagenomic in small intestine in mice

3.4.1. Differences in microflora between groups

The species richness in each sample was assessed at the levels of phylum, order, and species, and a distribution map illustrating species abundance at these corresponding taxonomic ranks was created.

As illustrated in Fig. 6A, 7A, and 8A, the similarity of bacterial community structures at the phylum, order, and species levels among samples from the control, WD, and HPRO groups was assessed using Principal Component Analysis (PCA). Significant alterations were detected in both the WD and HPRO

treatment groups. At all 3 taxonomy levels, substantial differences were found between samples from the control group and those from the WD group, indicating a marked divergence in bacterial community structure. Likewise, the bacterial communities present in samples from the WD and HPRO groups exhibited distinct characteristics. The findings indicated that WD significantly modified the framework of bacterial communities in mice, a change that was partially mitigated by the HPRO intervention.

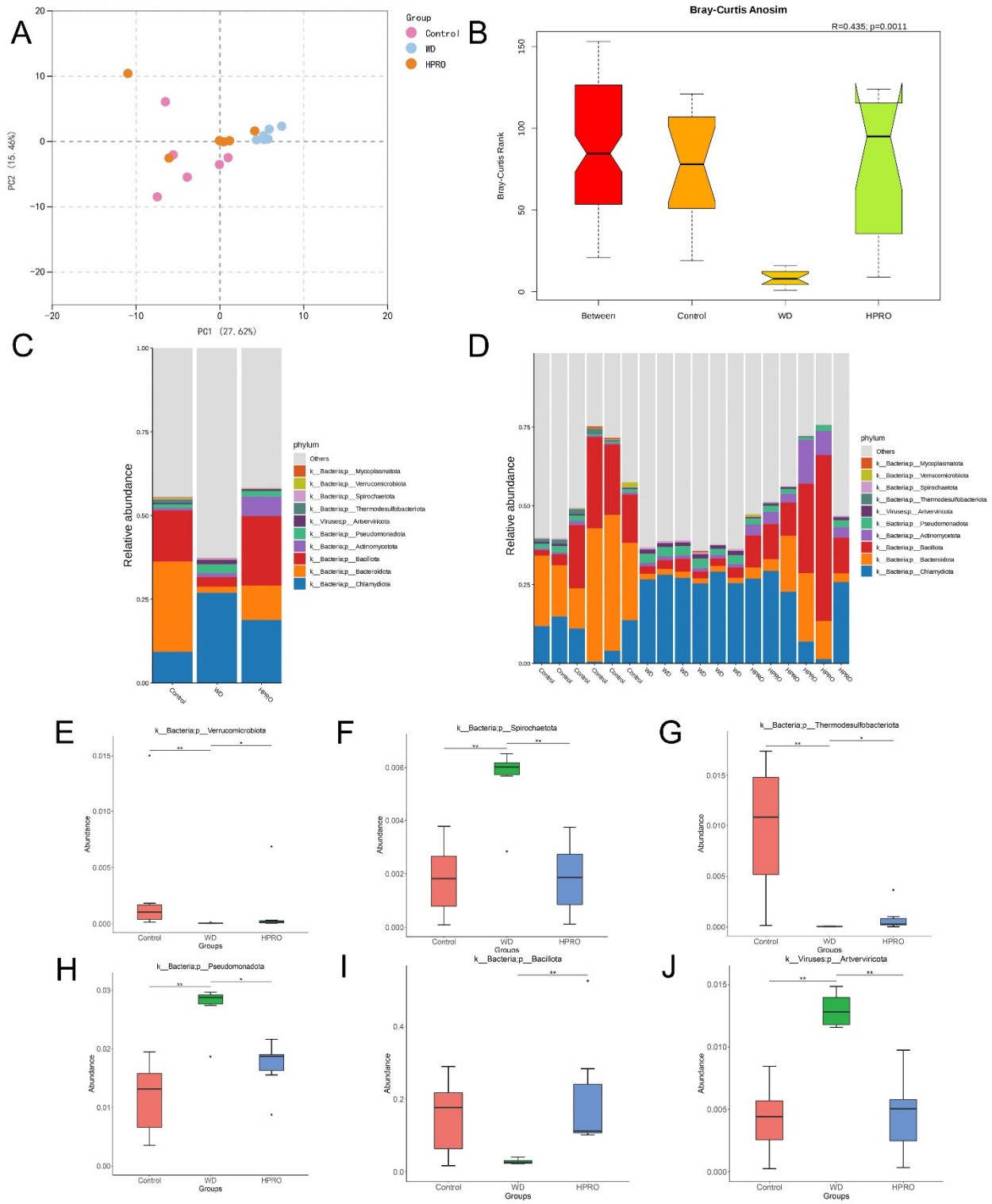

Fig. 6. Microbiota compositions at the phylum level. (A) PCA results from the similarities in bacterial community structures at the phylum level. (B) Analysis of Anosim based on phylum level. (C, D) Histogram of relative abundance at the phylum level. (E–J) Relative content of *Verrucomicrobiota*, *Spirochaetota*, *Thermodesulfobacteriota*, *Pseudomonadota*, *Bacillota*, and *Artverviricota* at the phylum level. * $P < 0.05$; ** $P < 0.01$.

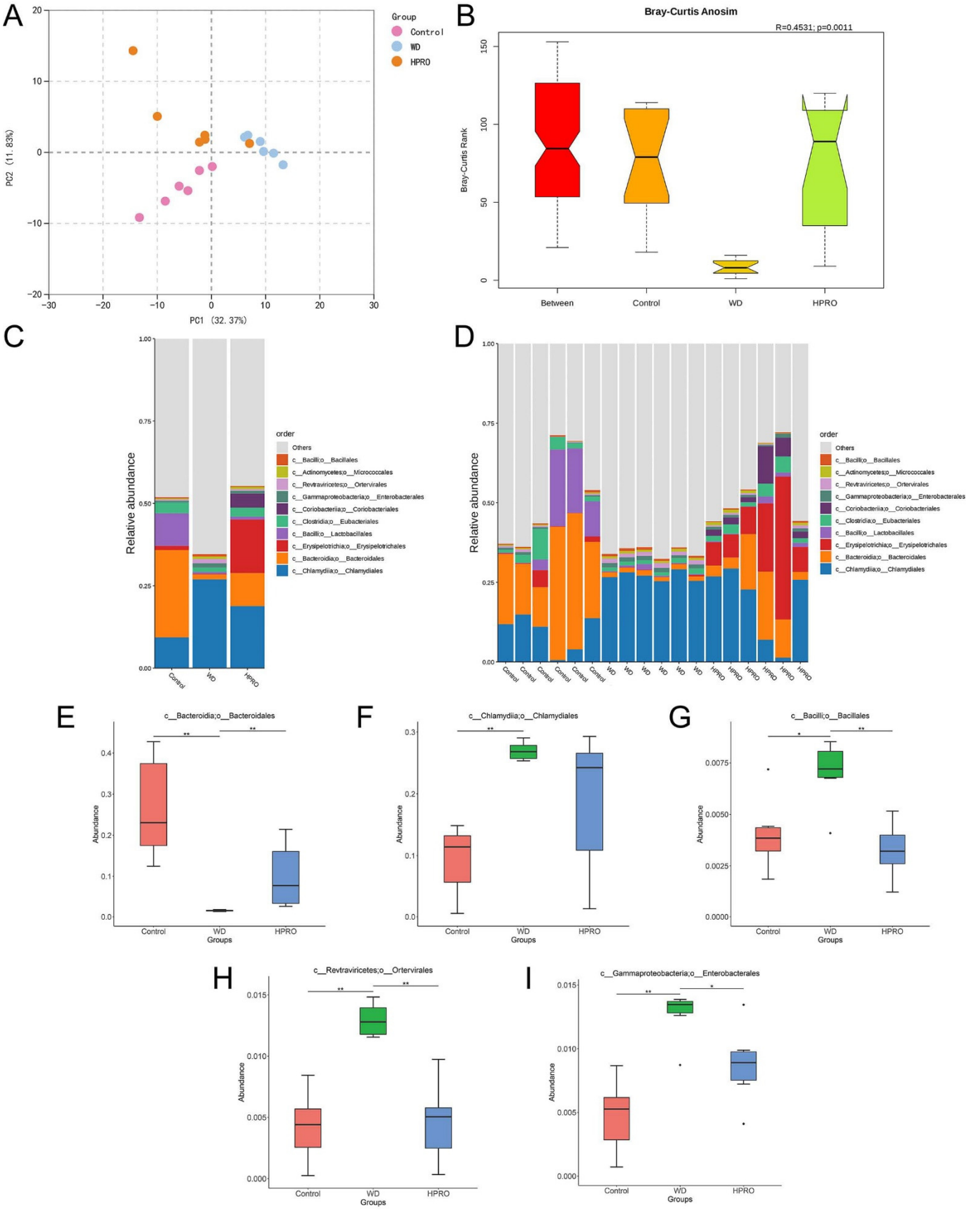

Fig. 7. Microbiota compositions at the order level. (A) PCA results from the similarities in bacterial community structures at the order level. (B) Analysis of Anosim based on order level. (C, D) Histogram of relative abundance at the order level. (E–J) Relative content of *Bacteroidales*, *Chlamydiales*, *Bacillales*, *Ortervirales*, and *Enterobacterales* at the order level. * $P < 0.05$; ** $P < 0.01$.

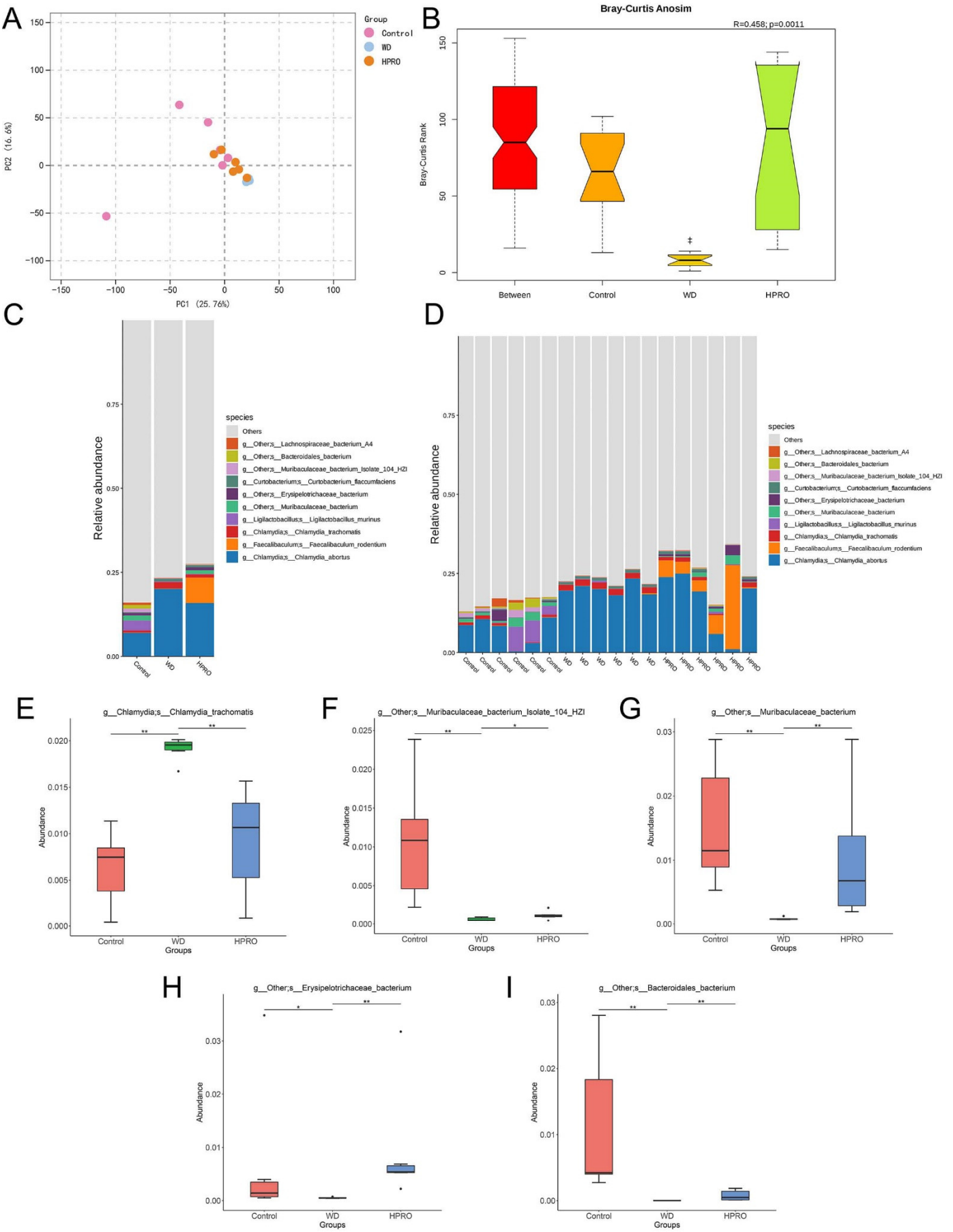

Fig. 8. Microbiota compositions at the species level. (A) PCA results from the similarities in bacterial community structures at the genus level. (B) Analysis of Anosim based on genus level. (C, D) Histogram of relative abundance at the genus level. (E–I) Relative content of *Chlamydia_trachomatis*, *Muribaculaceae_bacterium_Isolate_104_HZl*, *Muribaculaceae_bacterium*, *Erysipelotrichaceae_bacterium*, and *Bacteroidales_bacterium* at the species level. * $P < 0.05$; ** $P < 0.01$.

According to Fig. 6B, 7B, and 8B, Anosim analysis was employed to determine if the disparities within bacterial colonies across groups were significantly exceeding the differences observed within groups, specifically at the phylum, order, and species levels. An r value exceeding 0 suggests that the distinction between groups is more pronounced than that within groups. Conversely, when R is less than 0, it indicates that the within-group difference is more prominent than the between-group difference.

A *p*-value of less than 0.05 was deemed statistically significant. Significant differences in bacterial communities between the groups were observed at the phylum, order, and species levels, with correlation coefficients of R=0.435 (p=0.0011), R=0.4531 (p =0.0011), and R=0.4206 (p =0.0011).

The histograms display the abundance of the top 10 species classified by phylum, order, and genus levels. At the phylum level, as shown in Fig. 6C and D, Chlamydia had the largest abundance fraction, followed by *Bacteroidota*, *Bacillota*, et al. In Fig. 6E, F, G, H, I, and J, in comparison to the control group, the abundance of *Verrucomicrobiota*, *Thermodesulfobacteriota*, and *Bacillota* was significantly reduced, the abundance of *Spirochaetota*, *Pseudomonadota*, *Artverviricota* was significantly increased, in the WD group. Compared with the WD group, the HPRO group reversed this trend. Above all, the results suggest that *Pseudomonadota* might be the key phylum in the mitigation effect of HPRO.

At the order level of Fig. 7C and D, *Chlamydiales* had the highest abundance fraction, followed by *Bacteroidales* and *Erysipelotrichales*. Fig. 7E and 7I, compared with the control group, the abundance of *Bacteroidales*, decreased significantly, and *Chlamydiales*, *Enterobacterales*, *Ortervirales*, and *Bacillales* increased, in the WD group. Compared with the WD group, the HPRO group reversed this trend. Above all, the results suggest that *Enterobacterales* might be the key order in the mitigation effect of HPRO.

At the species level of Fig.8C and D, *Chlamydia_abortus* had the highest abundance fraction, followed by *Faecalibaculum_rodentium* and *Chlamydia_trachomatis*. In Fig. 8E and I, compared with the control group, WD treatment significantly decreased *Muribaculaceae_bacterium_lsolate_104_HZI*, *Muribaculaceae_bacterium*, *Erysipelotrichaceae_bacterium*, *Bacteroidales_bacterium* abundance, the abundance of *Chlamydia_trachomatis* was significantly increased. Compared with the WD group, the HPRO group reversed this trend.

In Fig.S1A (supplement file), linear discriminant analysis (LDA) coupled with the effect size measure (LEfSe) was utilized to discern variations in bacterial community composition serving as biomarkers distinguishing the control group from the WD group and the WD group from the HPRO group. The different colors-red, blue, and green-correspond to the control, WD, and HPRO groups, respectively. A statistically significant difference was observed for LDA > 2 between the groups. An elevated LDA value signifies a more substantial impact on the disparity between groups, suggesting that this flora serves as a more essential biomarker. *c_Bacteroidia*, *o_Bacteroidales*, and *p_Bacteroidota* were the species with relatively high abundance in the control group. *p_Chlamydiota*, *c_Chlamydiia*, and *g_Chlamydia* were relatively highly abundant in the WD group. *p_Bacillota*, *o_Erysipelotrichales*, and *c_Erysipelotrichia* were relatively abundant in the HPRO group. LEfSe was utilized to examine the biomarker microbiota exhibiting significant

differences between various groups. Fig. S1B (supplement file) illustrates 6 taxonomic levels ranging from phylum to species, *k_Bacteria*; *p_Bacillota*; *c_Erysipelotrichia*; *o_Erysipelotrichales*; *f_Erysipelotrichaceae*, there were significant differences in HPRO ($P < 0.01$). Species exhibiting significant alterations in HPRO are categorized within the *Bacillota* phylum. Therefore, these results suggest that HPRO improves AS in mice mainly by altering *Bacillota* in the small intestine.

3.4.2. Functional level of metagenomic sequences

In Fig. S1 C, D, E, F, and G (supplement file), 5 systems for functional annotation are employed: eggNOG, KEGG, CAZy, CARD, and GO. The results of functional annotation from eggNOG indicated that certain genes participated in the transport and metabolism of lipids, as well as in the production and conversion of energy.

Based on KEGG functional annotation (Fig. S1D, supplement file), some genes in Organismal Systems, Metabolism, Human Diseases, Genetic Information Processing, Environmental Information Processing, Cellular Processes, and other aspects were enriched. Fig. S1G (supplement file) shows: CAZy database annotations, according to the results of Glycoside Hydrolases, Glycosyl Transferases, and Carbohydrate-Binding Modules, these are the first 3 kinds of Carbohydrate enzymes. Fig. S1F (supplement file) shows the comment CARD database, according to the results of Mosaic tetracycline hold gene and ribosomal protection, protein, and beta-lactamase corresponding resistance gene of relative content is higher; this was followed by the membrane fusion protein of the multidrug efflux complex AdeFGH.

In Fig. S1E (supplement file), the Gene Ontology (GO) classifies terms into 3 main categories: biological processes, cellular components, and molecular functions. To assess if there were significant differences in functionality across the various groups, we employed the Kruskal-Wallis test to evaluate the hypothesis regarding the functional abundance data among the groups. We calculated *p*-values, defining $P < 0.05$ as indicative of significance. The functions exhibiting significant differences were then filtered based on these *p*-values. The boxplot displaying the significant functions from eggNOG can be found in Fig. S1C (supplement file). In KEGG, the boxplots of significant difference functions are shown in Fig. S1H, I, J, K, L, and M (supplement file). The results show that the function significant differences mainly Human_Diseases, Metabolism, Organismal_Systems, Cellular_Processes, Genetic_Information_Processing, and environmental L_Information_Processing, etc. As shown in Fig. S1N, O, P, Q, R, and S (supplement file), these results indicate that the functions with significant differences were Lipid_transport_and_metabolism, Amino_acid_transport_and_metabolism, Carbohydrate_transport_and_metabolism, Secondary_metabolites_biosynthesis_transport_and_catabolism, Energy_production_and_conversion and Signal_transduction_mechanisms, etc.

3.5. Correlation analysis of intestinal microbiota, liver lipids, and AS parameters in mice

Based on the results of taking the top 20 for lipids fixation and the top 50 for microorganisms by default, an association heat map was drawn.

Previous studies have reported correlations between liver lipids and microbiota [57]. Lipidomics findings indicated that, when contrasted with the control group, the levels of PE (22:2_18:0) and PA (20:2_22:5) in the WD group exhibited a significant decrease ($P < 0.01$). Conversely, the HPRO group demonstrated a significant increase in these contents ($P < 0.01$). As illustrated in Fig. 9A, the joint analysis at the phylum level revealed that the levels of *k_Bacteria*, *f_Muribaculaceae*, *c_Bacteroidia*, *o_Bacteroidales* and *p_Bacteroidota* showed a positive correlation with the levels of PE (22:2_18:0) and PA (20:2_22:5) ($P < 0.01$), and negatively correlated with the concentrations of various other lipids. The levels of *g_Chlamydia*, *f_Chlamydiaceae*, *o_Chlamydiales*, *p_Chlamydiota*, *c_Chlamydiia*, *s_Chlamydia_abortus* were significantly negatively correlated with the concentrations of PE (22:2_18:0) and PA (20:2_22:5) ($P < 0.05$), and positively correlated with the concentrations of other lipids.

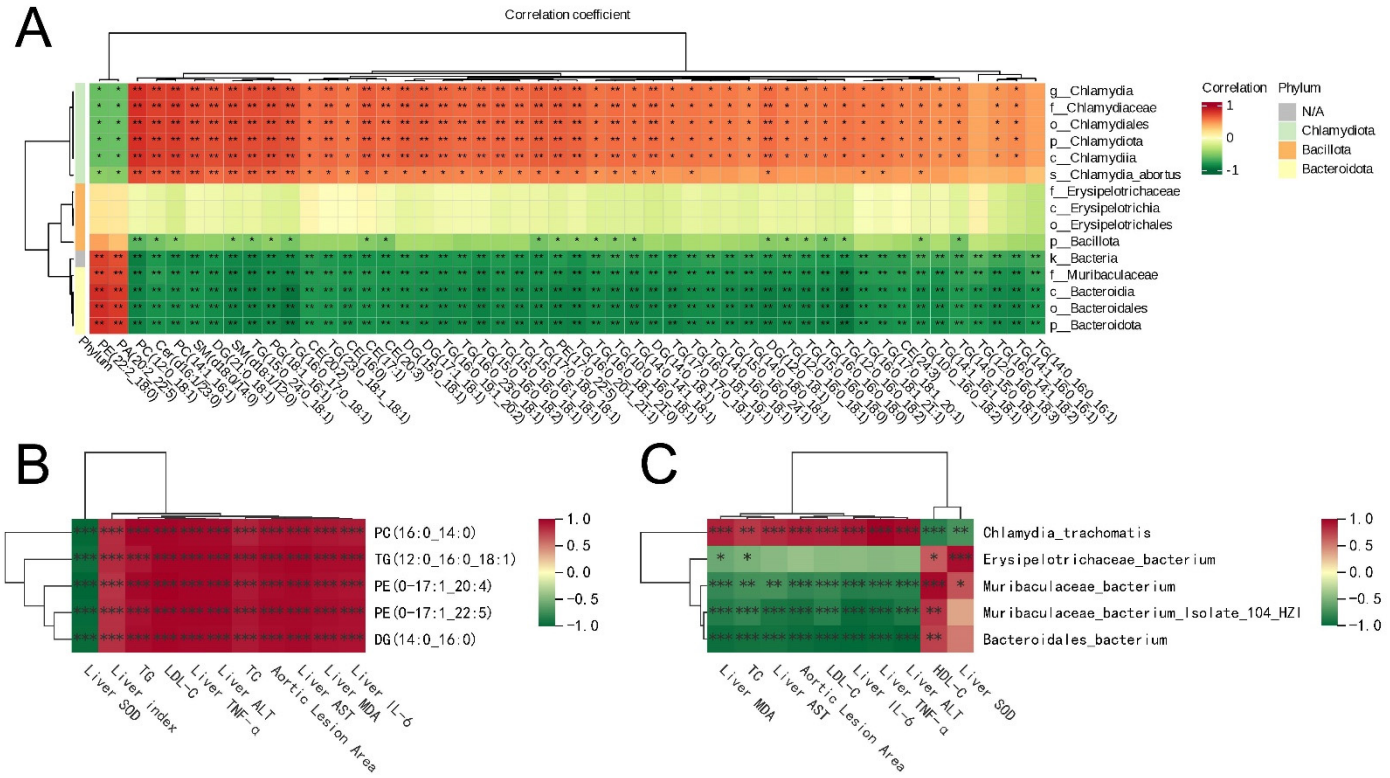

Fig. 9. Metagenomics, lipidomics, and parameters of AS heat map. (A) Correlation analysis between the intestine microbiome at the phylum level and identified lipids. (B) Pearson correlation between identified lipids and parameters of AS. (C) Spearman correlation analysis between the intestine microbiome at species levels and parameters of AS. Red shows a positive correlation, while green shows a negative correlation. The darker the color, the stronger the correlation. The closer the color is to white, the closer the correlation is to zero. * $P < 0.05$; ** $P < 0.01$; *** $P < 0.001$.

HPRO significantly changed the composition and abundance of intestinal microbiota and liver lipids in WD-induced ApoE$^{-/-}$ mice and reduced aortic atherosclerotic area, lipid levels, liver index, oxidative stress, inflammation, and injury indexes. To ascertain whether these remits were associated with intestine microbiota and liver lipids, Spearman and Pearson correlation analyses were performed, respectively. In order to elucidate the correlation between intestinal microbiota, Liver lipids, and AS parameters (Aortic Lesion Area, TC, LDL-C, HDL-C, TG, Liver index, Liver SOD, Liver MDA, liver TNF-α, Liver IL-6, Liver ALT, and Liver AST). As shown in Fig. 9B, additional correlational analyses were conducted to examine the potential association between the lipids with the most significant difference and AS-related symptoms. PC (16:0_14:0),

TG (12:0_16:0 _18:1), PE (0-17:1 _20:4), PE (0-17:1 _22:5), DG (14:0 _16:0) were positively correlated with Liver index, Liver MDA, Liver TNF-α, Liver IL-6, Liver ALT, Liver AST, TC, Aortic Lesion Area, LDL-C and TG, and inversely associated with Liver SOD. In comparison to the control group, the WD group increased the expression of these lipids, and the HPRO group reversed this trend. HPRO may contribute to reducing AS through these lipids. In Fig. 9C, Microbiota at Phylum level, *Chlamydia_trachomatis* was positively correlated with Liver MDA, TC, Liver AST, Aortic Lesion Area, LDL-C, Liver IL-6, Liver TNF-α, and Liver ALT. It was negatively correlated with HDL-C and Liver SOD. *Erysipelotrichaceae_bacterium*, *Muribaculaceae_bacterium*, *Muribaculaceae_bacterium_Isolate_104_HZI*, and *Bacteroidales_bacterium*, these parameters were negatively correlated with HDL-C and positively correlated with Liver SOD. The results suggest that *Muribaculaceae* might be the key species in the mitigation effect of HPRO. In summary, our results suggest that intestine microbiota and liver lipids are intricately associated with AS parameters, and their composition and availability may significantly influence the occurrence and advancement of AS, which is consistent with the results of previous studies [58-62].

4. Discussion

AS-related cardiovascular diseases have garnered international attention due to their high incidence of disease prevalence and death rate. In recent decades, a substantial number of epidemiological, clinical, and experimental research efforts have demonstrated that dietary factors are crucial in preventing the onset of AS [3]. Recognized as a vital natural active compound, β-sitosterol has received considerable interest owing to its role in the prophylaxis and management of AS. One of the primary ways that phytosterols contribute to cholesterol reduction is through their ability to impede the absorption of cholesterol within the intestinal tract. Consequently, when phytosterols are ingested in conjunction with meals, they effectively block the uptake of dietary cholesterol from the intestine right at the outset, thereby significantly enhancing their efficacy in lowering TC and LDL-C levels [23]. The WD ApoE$^{-/-}$ mice model is commonly utilized in studies of AS, exhibiting elevated serum levels of TG, TC, and LDL-C. These component-TG, TC, and LDL-C are linked to an increased risk of developing AS [63, 64]. As a result, controlling lipid levels offers a promising strategy for tackling AS. In this investigation, mice deficient in ApoE$^{-/-}$ mice that were given a WD exhibited heightened levels of serum TG, TC, and LDL-C, while simultaneously showing reduced levels of HDL. Nonetheless, the feeding of HPRO led to a decline in serum TG, TC, and LDL-C in ApoE$^{-/-}$ mice. Prior research has indicated that β-sitosterol has an anti-atherosclerotic effect, which is achieved by lowering TC and TG levels in these ApoE$^{-/-}$ mice [65]. In dyslipidemia, the lipid level is increased and the antioxidant capacity is decreased, which is manifested as severe lipid peroxidation and a high risk of AS. MDA is the end product of lipid peroxidation and an important index reflecting the level of lipid peroxidation in the body [66, 67]. Studies have shown that MDA is involved in the pathogenesis of AS and promotes plaque formation [68]. For example, baicalin lowers the concentrations of IL-6, TNF-α, and MDA through the NF-κB signaling pathway, aiding in the alleviation of AS [69]. This study suggests that HPRO lowers blood lipid levels and reduces MDA production, implying

that the positive effect of HPRO on AS may be closely linked to lower lipid levels and a reduction in lipid peroxidation.

AS is recognized as a persistent inflammatory disorder marked by the thickening of the intimal layer and the development of plaques [70]. During the progression of AS, there is a significant release of inflammatory cytokines that accelerate both the initiation and progression of atherosclerotic lesions [71]. TNF-α is acknowledged as a proinflammatory cytokine that plays a role in inflammatory disturbances observed at several stages of AS [72]. Similarly, IL-6 is identified as a significant risk factor facilitating the emergence of chronic inflammation and the development of atherosclerotic plaques [73]. Meanwhile, inflammatory markers have been utilized as critical indicators of AS. As a result, we explored the effects of HPRO on the manufacture of proinflammatory cytokines within the ApoE$^{-/-}$ mice model. Our findings revealed the concentrations of TNF-α and IL-6 in the liver tissues of mice on a WD were heightened in comparison to the control group. Furthermore, we demonstrated that treatment with HPRO reduced atherosclerotic inflammation by lowering the levels of inflammatory markers.

Obesity constitutes a significant risk factor for AS and serves a significant function [74, 75]. Rapeseed oil consumption leads to a substantial decrease in body weight in comparison to SFAs [76]. In this research, we found that WD resulted in increased body weight, liver index, and WAT in ApoE$^{-/-}$ mice relative to those C57BL/6J mice that were kept on a normal diet. Furthermore, our results showed that HPRO contributed to a decrease in body weight, liver index, and WAT, alongside a reduction in adipocyte area in ApoE$^{-/-}$ mice. These results suggest that HPRO might have properties that combat obesity. It serves as the primary place for lipid storage in the organism and may serve as an indicator of antiobesity effects [77]. Obesity caused by a diet rich in fats can increase the accumulation of lipids in the eWAT. Investigations centering on WAT have become an important field in the research of antiobesity strategies [78]. The oil derived from kiwifruit seeds may help fight fat by affecting heat production and the intestine microbiome in C57BL/6 mice that have become obese as a result of a high-fat diet [79]. Nonetheless, the influence of HPRO on lipid metabolism mechanisms within the WAT of ApoE$^{-/-}$ mice remains inadequately explored. The aforementioned findings suggest that HPRO can considerably decrease both the WAT and lipid buildup in WAT. Problems with the breakdown of fats are crucial contributors to the onset of AS. The liver, as the body's biggest organ for metabolism, is pivotal in lipid metabolism as it regulates fat synthesis, lipolysis, as well as the absorption and release of serum lipoproteins. A lot of therapeutic and experimental research has indicated that disruptions in liver lipid metabolism are intimately linked with AS development, and abnormalities in this metabolic function may increase the risk of AS emerging [80]. AMPK is essential for the regulation of the metabolic conversion of energy and can influence the expression of critical elements that are engaged in the creation of mitochondria and the use of energy [81]. Studies have shown that activating AMPK could decrease lipid buildup by regulating key lipogenic genes [82, 83]. What we found suggests that D-HPRO significantly improves the p-AMPK/AMPK ratio. Notably, the AMPK downstream targets-SREBP-1, ACC, and FASN-are all implicated in lipid metabolism and contribute to the buildup of lipids in WAT [82]. The current research

indicates that HPRO may decrease both lipid synthesis and accumulation in WAT by stimulating AMPK in the liver, which subsequently leads to the down-regulation of its downstream transcription factors, SREBP-1 and FASN, thereby mitigating AS.

The two-way interaction relationship between the intestine and the liver, often referred to as the "intestine-liver axis," has been identified as a mechanism influencing the onset and progression of AS [84]. An expanding corpus of research has demonstrated that intestinal bacteria serve a significant function in governing metabolic function and energy balance, and they are thought to be involved in the progression of AS through the intestine-liver axis [85-87]. In this study, we found that HPRO can play a role in preventing AS by regulating the *Pseudomonadota* at the phylum level, the *Enterobacterales* at the order level, and the *Muribaculaceae* at the species level, which have also been reported to be closely associated with the development of AS. At the phylum level, according to reports, AS regulation by *Pseudomonadota* occurs through the degradation of purine [88]. At the order level, *Enterobacterales* bacteria have been involved in the development of AS [89]. At the species level, Literature has shown that *Muribaculaceae* is a kind of anti-inflammatory beneficial bacteria. Highland barley supplementation may reduce the building up of arterial plaque by increasing the abundance of *Muribaculaceae* and other bacteria and synthesizing anti-inflammatory metabolites from intestinal microbiota [90]. Mulberry anthocyanins alleviate dextran sulfate sodium (DSS)-induced colitis by augmenting the abundance of *Muribaculaceae* [91]. *Clostridioides* difficile aggravates DSS-induced colitis by reducing the proportions of *Muribaculaceae*, shaping the intestinal flora, and promoting phagocyte aggregation [92]. Phlorizin Mitigates Colitis in mice by increasing the concentrations of advantageous microorganisms *Muribaculaceae*, modulating intestinal microbiota, and inhibiting ferroptosis [93]. All of these studies support our findings, that HPRO is achieved by increasing the prevalence of beneficial bacteria *Bacillota* and *Muribaculaceae* while decreasing the prevalence of the harmful bacteria *Enterobacterales* and *Pseudomonadota* to prevent AS.

Regrettably, our research has specific limitations, including the fact that experiments were conducted solely at the cellular and murine levels without any trials involving humans. While we examined the connection between the positive impact of HPRO on the intestine bacteria and the decrease in AS deterioration, additional validation studies are necessary to illustrate the direct correlation between HPRO, intestinal flora, and AS. In our upcoming investigations, we will take these elements into account and enhance our approach.

5. Conclusions

In conclusion, HPRO reduced serum TC, TG, and LDL-C content, increased HDL-C content, reduced lipid deposition in arterial walls, and reduced plaque area. Meanwhile, by reducing ROS levels, oxidative stress was reduced, and aortic AS status was relieved. Liver lipidomics analysis and subsequent experiments with ApoE$^{-/-}$ mice and HepG2 cells suggested that HPRO may affect the expression of SREBP-1 and FASN, which are related to lipogenesis, through AMPK regulation, and improve lipid-lowering and protect the liver in HepG2 cells. Moreover, HPRO showed better lipid-lowering and protective effects than β-sitosterol in

HepG2 cells. In small intestinal metagenic analysis, HPRO regulated the abundance of microbiota including *Bacillota*, *Pseudomonadota*, *Enterobacterales*, and *Muribaculaceae*, reducing problems with the structure of microbiota abundance in mice. The correlation analysis among liver lipids, intestinal flora, and AS indexes found a significant relationship among the three. As can be seen, in a mouse model of AS, HPRO intake can significantly reduce aortic plaque and lipid concentrations, reduce oxidative stress and inflammation, and support the balance of liver lipid composition and intestinal flora, thereby preventing AS injury. In addition, significant reductions in aortic microstructure and aging also point to the location of HPRO's effects. Therefore, subsequent studies need to verify the role of HPRO in preventing AS in humans and explore the synergistic effects and influence mechanisms of various beneficial components of HPRO *in vivo*. This study provides the theoretical basis and technical guidance for employing HPRO AS an edible oil to prevent AS.

Acknowledgements

This work was supported by the National Key Research and Development Project of China (2021YFD1600101), Basic Research Center, Innovation Program of Chinese Academy of Agricultural Sciences(CAAS-BRC-FNH-2025-03), the National Natural Science Foundation of China (32302092), the Nature Science Foundation of Hubei Province (2023AFB314), the Major Project of Hubei Hongshan Laboratory (2022hszd002), the earmarked fund for the China Agriculture Research System (CARS-12), and the Agricultural Science and Technology Innovation Program of Chinese Academy of Agricultural Sciences (CAAS-ASTIP-2025-OCRI).

Declaration of Interest statement

The authors declare that they have no known competing financial interests or personal relationships that could have appeared to influence the work reported in this paper.

Reference

[1] J.L. Björkegren, A.J. Lusis, Atherosclerosis: recent developments, Cell. 185 (2022) 1630-1645. https://doi.org/10.1016/j.cell.2022.04.004.

[2] P. Libby, The changing landscape of atherosclerosis, Nature. 592 (2021) 524-533. https://doi.org/10.1038/s41586-021-03392-8.

[3] N. Torres, M. Guevara-Cruz, L.A. Velázquez-Villegas, et al., Nutrition and Atherosclerosis, Arch Med Res. 46 (2015) 408-426. https://doi.org/10.1016/j.arcmed.2015.05.010.

[4] Y. Zhao, Y. Yang, R. Xing, et al., Hyperlipidemia induces typical atherosclerosis development in Ldlr and Apoe deficient rats, Atherosclerosis. 271 (2018) 26-35. https://doi.org/https://doi.org/10.1016/j.atherosclerosis.2018.02.015.

[5] P.-P. He, T. Jiang, X.-P. OuYang, et al., Lipoprotein lipase: Biosynthesis, regulatory factors, and its role in atherosclerosis and other diseases, Clinica Chimica Acta. 480 (2018) 126-137. https://doi.org/https://doi.org/10.1016/j.cca.2018.02.006.

[6] F.J. Field, N.T. Kam, S.N. Mathur, Regulation of cholesterol metabolism in the intestine, Gastroenterology. 99 (1990) 539-551. https://doi.org/10.1016/0016-5085(90)91040-d.

[7] S. Abumweis, R. Barake, P. Jones, Plant sterols/stanols as cholesterol lowering agents: a meta-analysis of randomized controlled trials, Food Nutr Res. 52 (2008) 1811. https://doi.org/10.3402/fnr.v52i0.1811.

[8] J.W. Yang, H.F. Ji, Phytosterols as bioactive food components against nonalcoholic fatty liver disease, Crit Rev Food Sci Nutr. 63 (2023) 4675-4686. https://doi.org/10.1080/10408398.2021.2006137.

[9] L. Song, H. Zhou, W. Yu, et al., Effects of Phytosterol Ester on the Fatty Acid Profiles in Rats with Nonalcoholic Fatty Liver Disease, J Med Food. 23 (2020) 161-172. https://doi.org/10.1089/jmf.2019.4468.

[10] A. Brodkorb, L. Egger, M. Alminger, et al., INFOGEST static in vitro simulation of gastrointestinal food digestion, Nat Protoc. 14 (2019) 991-1014. https://doi.org/10.1038/s41596-018-0119-1.

[11] W.-K. Wu, E.A. Ivanova, A.N. Orekhov, Gut microbiome: A possible common therapeutic target for treatment of atherosclerosis and cancer, Semin. Cancer Biol. 70 (2021) 85-97. https://doi.org/https://doi.org/10.1016/j.semcancer.2020.06.017.

[12] A.L. Jonsson, F. Bäckhed, Role of gut microbiota in atherosclerosis, Nat. Rev. Cardiol. 14 (2017) 79-87. https://doi.org/10.1038/nrcardio.2016.183.

[13] Q. Zhang, L. Zhang, C. Chen, et al., The gut microbiota-artery axis: A bridge between dietary lipids and atherosclerosis?, Prog Lipid Res. 89 (2023) 101209. https://doi.org/10.1016/j.plipres.2022.101209.

[14] M. Schoeler, R. Caesar, Dietary lipids, gut microbiota and lipid metabolism, Rev Endocr Metab Disord. 20 (2019) 461-472. https://doi.org/10.1007/s11154-019-09512-0.

[15] M.-l. Chen, L. Yi, Y. Zhang, et al., Resveratrol Attenuates Trimethylamine-N-Oxide (TMAO)-Induced Atherosclerosis by Regulating TMAO Synthesis and Bile Acid Metabolism via Remodeling of the Gut Microbiota, mBio. 7 (2016) 10.1128/mbio.02210-02215. https://doi.org/10.1128/mbio.02210-15.

[16] M. Zhang, Z. Xie, W. Gao, et al., Quercetin regulates hepatic cholesterol metabolism by promoting cholesterol-to-bile acid conversion and cholesterol efflux in rats, NUTR RES. 36 (2016) 271-279. https://doi.org/https://doi.org/10.1016/j.nutres.2015.11.019.

[17] L. Ding, L.-Y. Zhang, H.-H. Shi, et al., Eicosapentaenoic Acid-Enriched Phosphoethanolamine Plasmalogens Alleviated Atherosclerosis by Remodeling Gut Microbiota to Regulate Bile Acid Metabolism in LDLR–/– Mice, Agric. Food Chem. 68 (2020) 5339-5348. https://doi.org/10.1021/acs.jafc.9b08296.

[18] C. Fernández, Y. Suárez, A.J. Ferruelo, et al., Inhibition of cholesterol biosynthesis by Δ22-unsaturated phytosterols via competitive inhibition of sterol Δ24-reductase in mammalian cells, BIOCHEM J. 366 (2002) 109-119. https://doi.org/10.1042/bj20011777.

[19] C.-h. Zhao, C. Zhao, H.-q. Ye, et al., Hypolipidemic activity of low-cholesterol ovum oil of Rana chensinensis and phytosterol (stigmasterol) in rats, J. Zhejiang Univ. Sci. B. 20 (2019) 613. https://doi.org/10.1631/jzus.B1900018.

[20] H.-L. Yu, L.-F. Gao, W.-W. Ma, et al., The effects of phytosterol supplementation on serum LDL-C levels and learning ability in mice fed a high-fat, high-energy diet from gestation onward, INT J FOOD SCI NUTR. 64 (2013) 724-729. https://doi.org/10.3109/09637486.2013.787396.

[21] S.C. Chen, J.T. Judd, M. Kramer, et al., Phytosterol intake and dietary fat reduction are independent and additive in their ability to reduce plasma LDL cholesterol, Lipids. 44 (2009) 273. https://doi.org/10.1007/s11745-008-3278-y.

[22] R. Yang, L. Xue, L. Zhang, et al., Phytosterol Contents of Edible Oils and Their Contributions to Estimated Phytosterol Intake in the Chinese Diet, Foods. 8 (2019) 334. https://www.mdpi.com/2304-8158/8/8/334.

[23] A.M. Doornbos, E.M. Meynen, G.S. Duchateau, et al., Intake occasion affects the serum cholesterol lowering of a plant sterol-enriched single-dose yoghurt drink in mildly hypercholesterolaemic subjects, Eur J Clin Nutr. 60 (2006) 325-333. https://doi.org/10.1038/sj.ejcn.1602318.

[24] L. Lin, H. Allemekinders, A. Dansby, et al., Evidence of health benefits of canola oil, Nutr Rev. 71 (2013) 370-385. https://doi.org/10.1111/nure.12033.

[25] I. Ilyas, P.J. Little, Z. Liu, et al., Mouse models of atherosclerosis in translational research, Trends Pharmacol. Sci. 43 (2022) 920-939. https://doi.org/https://doi.org/10.1016/j.tips.2022.06.009.

[26] Li, Y., Yu, Z., Liu, Y., Wang, T., Liu, Y., Bai, Z., Ren, Y., Ma, H., Bao, T., Lu, H., Wang, R., Yang, L., Yan, N., Yan, R., Jia, S., Zhang, X., & Wang, H. (2022). Dietary α-Linolenic Acid-Rich Flaxseed Oil Ameliorates High-Fat Diet-Induced Atherosclerosis via Gut Microbiota-Inflammation-Artery Axis in ApoE (-/-) Mice. Front Cardiovasc Med, 9, 830781. https://doi.org/10.3389/fcvm.2022.830781.

[27] A. Brodkorb, L. Egger, M. Alminger, et al., INFOGEST static in vitro simulation of gastrointestinal food digestion, Nat Protoc. 14 (2019) 991-1014. https://doi.org/10.1038/s41596-018-0119-1.

[28] F. Xu, L. Wang, X. Ju, et al., Transepithelial Transport of YWDHNNPQIR and Its Metabolic Fate with Cytoprotection against Oxidative Stress in Human Intestinal Caco-2 Cells, Agric. Food Chem. 65 (2017) 2056-2065. https://doi.org/10.1021/acs.jafc.6b04731.

[29] F. Vahid, P. Krischler, B. Leners, et al., Effect of Digested Selected Food Items on Markers of Oxidative Stress and Inflammation in a Caco-2-Based Human Gut Epithelial Model, Antioxidants (Basel). 13 (2024) https://doi.org/10.3390/antiox13020150.

[30] Y. Liu, X. Yang, J. Gan, et al., CB-Dock2: improved protein–ligand blind docking by integrating cavity detection, docking and homologous template fitting, Nucleic Acids Res. 50 (2022) W159-W164. https://doi.org/10.1093/nar/gkac394.

[31] X. Yang, Y. Liu, J. Gan, et al., FitDock: protein–ligand docking by template fitting, Briefings Bioinf. 23 (2022) https://doi.org/10.1093/bib/bbac087.

[32] F. Lovren, H. Teoh, S. Verma, Obesity and atherosclerosis: mechanistic insights, Can J Cardiol. 31 (2015) 177-183. https://doi.org/10.1016/j.cjca.2014.11.031.

[33] X. Zhang, Y. Zhang, P. Wang, et al., Adipocyte Hypoxia-Inducible Factor 2α Suppresses Atherosclerosis by Promoting Adipose Ceramide Catabolism, Cell Metab. 30 (2019) 937-951.e935. https://doi.org/10.1016/j.cmet.2019.09.016.

[34] A.D. van Dam, M.R. Boon, J.F.P. Berbée, et al., Targeting white, brown and perivascular adipose tissue in atherosclerosis development, Eur J Pharmacol. 816 (2017) 82-92. https://doi.org/10.1016/j.ejphar.2017.03.051.

[35] B.A. Ference, H.N. Ginsberg, I. Graham, et al., Low-density lipoproteins cause atherosclerotic cardiovascular disease. 1. Evidence from genetic, epidemiologic, and clinical studies. A consensus statement from the European Atherosclerosis Society Consensus Panel, Eur Heart J. 38 (2017) 2459-2472. https://doi.org/10.1093/eurheartj/ehx144.

[36] S. Raposeiras-Roubin, X. Rosselló, B. Oliva, et al., Triglycerides and Residual Atherosclerotic Risk, J Am Coll Cardiol. 77 (2021) 3031-3041. https://doi.org/10.1016/j.jacc.2021.04.059.

[37] J.F. Viles-Gonzalez, V. Fuster, J.J. Badimon, Links between inflammation and thrombogenicity in atherosclerosis, Curr Mol Med. 6 (2006) 489-499. https://doi.org/10.2174/156652406778018707.

[38] D.J. Tyrrell, M.G. Blin, J. Song, et al., Age-Associated Mitochondrial Dysfunction Accelerates Atherogenesis, Circ Res. 126 (2020) 298-314. https://doi.org/10.1161/circresaha.119.315644.

[39] D.J. Tyrrell, D.R. Goldstein, Ageing and atherosclerosis: vascular intrinsic and extrinsic factors and potential role of IL-6, Nat Rev Cardiol. 18 (2021) 58-68. https://doi.org/10.1038/s41569-020-0431-7.

[40] S.I. Bloom, M.T. Islam, L.A. Lesniewski, et al., Mechanisms and consequences of endothelial cell senescence, Nat Rev Cardiol. 20 (2023) 38-51. https://doi.org/10.1038/s41569-022-00739-0.

[41] G.P. Dimri, X. Lee, G. Basile, et al., A biomarker that identifies senescent human cells in culture and in aging skin in vivo, Proc Natl Acad Sci U S A. 92 (1995) 9363-9367. https://doi.org/10.1073/pnas.92.20.9363.

[42] M. Batty, M.R. Bennett, E. Yu, The Role of Oxidative Stress in Atherosclerosis, Cells. 11 (2022) https://doi.org/10.3390/cells11233843.

[43] R. Dawes, S. Petrova, Z. Liu, et al., Combinations of CD45 isoforms are crucial for immune function and disease, J Immunol. 176 (2006) 3417-3425. https://doi.org/10.4049/jimmunol.176.6.3417.

[44] E.C. Jury, P.S. Kabouridis, F. Flores-Borja, et al., Altered lipid raft-associated signaling and ganglioside expression in T lymphocytes from patients with systemic lupus erythematosus, J Clin Invest. 113 (2004) 1176-1187. https://doi.org/10.1172/jci20345.

[45] J.M. Penninger, J. Irie-Sasaki, T. Sasaki, et al., CD45: new jobs for an old acquaintance, Nat Immunol. 2 (2001) 389-396. https://doi.org/10.1038/87687.

[46] I. Perrotta, Ultrastructural features of human atherosclerosis, Ultrastruct Pathol. 37 (2013) 43-51. https://doi.org/10.3109/01913123.2011.592721.

[47] A. Milutinović, D. Šuput, R. Zorc-Pleskovič, Pathogenesis of atherosclerosis in the tunica intima, media, and adventitia of coronary arteries: An updated review, Bosn J Basic Med Sci. 20 (2020) 21-30. https://doi.org/10.17305/bjbms.2019.4320.

[48] T. Meng, X. Li, C. Li, et al., Natural products of traditional Chinese medicine treat atherosclerosis by regulating inflammatory and oxidative stress pathways, Front Pharmacol. 13 (2022) 997598. https://doi.org/10.3389/fphar.2022.997598.

[49] M. Cheraghi, H. Ahmadvand, A. Maleki, et al., Oxidative Stress Status and Liver Markers in Coronary Heart Disease, Rep Biochem Mol Biol. 8 (2019) 49-55.

[50] P. Adibi, M. Sadeghi, M. Mahsa, et al., Prediction of coronary atherosclerotic disease with liver transaminase level, Liver Int. 27 (2007) 895-900. https://doi.org/10.1111/j.1478-3231.2007.01545.x.

[51] C. Yue, M. Li, J. Li, et al., Medium-, long- and medium-chain-type structured lipids ameliorate high-fat diet-induced atherosclerosis by regulating inflammation, adipogenesis, and gut microbiota in ApoE(-/-) mice, Food Funct. 11 (2020) 5142-5155. https://doi.org/10.1039/d0fo01006e.

[52] H. Han, T. Xue, J. Li, et al., Plant sterol ester of α-linolenic acid improved non-alcoholic fatty liver disease by attenuating endoplasmic reticulum stress-triggered apoptosis via activation of the AMPK, J Nutr Biochem. 107 (2022) 109072. https://doi.org/10.1016/j.jnutbio.2022.109072.

[53] F. Ahmad, S. Abbas, A. Bibi, et al. Canola Oil as a Bio-additive: Properties, Processing and Applications. In: Bhawani S.A., A. Khan, M.N. Mohmad Ibrahim, et al., editors. Vegetable Oil-Based Composites: Processing, Properties and Applications. Singapore: Springer Nature Singapore; 2024, p. 59-85. https://doi.org/10.1007/978-981-99-9959-0_4.

[54] M.H. Abukhalil, O.E. Hussein, M. Bin-Jumah, et al., Farnesol attenuates oxidative stress and liver injury and modulates fatty acid synthase and acetyl-CoA carboxylase in high cholesterol-fed rats, Environ. Sci. Pollut. Res. 27 (2020) 30118-30132. https://doi.org/10.1007/s11356-020-09296-w.

[55] T. Chen, T. Wang, Y. Shi, et al., Integrated network pharmacology, metabolomics and molecular docking analysis to reveal the mechanisms of quercetin in the treatment of hyperlipidemia, J Pharm Biomed Anal. 252 (2025) 116507. https://doi.org/https://doi.org/10.1016/j.jpba.2024.116507.

[56] R. Jafari, H. Almqvist, H. Axelsson, et al., The cellular thermal shift assay for evaluating drug target interactions in cells, Nat Protoc. 9 (2014) 2100-2122. https://doi.org/10.1038/nprot.2014.138.

[57] X.-R. Lu, X.-W. Liu, S.-H. Li, et al., Untargeted lipidomics and metagenomics reveal the mechanism of aspirin eugenol ester relieving hyperlipidemia in ApoE−/− mice, Front. nutr. 9 (2022) https://doi.org/10.3389/fnut.2022.1030528.

[58] S. Ascher, C. Reinhardt, The gut microbiota: An emerging risk factor for cardiovascular and cerebrovascular disease, Eur J Immunol. 48 (2018) 564-575. https://doi.org/10.1002/eji.201646879.

[59] Y. Zhu, Q. Li, H. Jiang, Gut microbiota in atherosclerosis: focus on trimethylamine N-oxide, Apmis. 128 (2020) 353-366. https://doi.org/10.1111/apm.13038.

[60] S. Yang, X. Li, F. Yang, et al., Gut Microbiota-Dependent Marker TMAO in Promoting Cardiovascular Disease: Inflammation Mechanism, Clinical Prognostic, and Potential as a Therapeutic Target, Front Pharmacol. 10 (2019) 1360. https://doi.org/10.3389/fphar.2019.01360.

[61] N.S. Nurmohamed, J.M. Kraaijenhof, M. Mayr, et al., Proteomics and lipidomics in atherosclerotic cardiovascular disease risk prediction, Eur Heart J. 44 (2023) 1594-1607. https://doi.org/10.1093/eurheartj/ehad161.

[62] F. Eichelmann, L. Sellem, C. Wittenbecher, et al., Deep Lipidomics in Human Plasma: Cardiometabolic Disease Risk and Effect of Dietary Fat Modulation, Circulation. 146 (2022) 21-35. https://doi.org/10.1161/circulationaha.121.056805.

[63] J. Xu, C. Ma, M. Chen, et al., Lipingshu capsule improves atherosclerosis associated with lipid regulation and inflammation inhibition in apolipoprotein E-deficient mice, Lipids Health Dis. 17 (2018) 182. https://doi.org/10.1186/s12944-018-0823-4.

[64] H. Liu, X. Li, Y. Song, et al., MicroRNA-217 attenuates intima-media complex thickness of ascending aorta measured by ultrasound bio-microscopy and inhibits inflammation and lipid metabolism in atherosclerotic models of ApoE(-/-) mice, Lipids Health Dis. 17 (2018) 170. https://doi.org/10.1186/s12944-018-0825-2.

[65] S. Jiang, K. Gao, F. Zhang, et al., β-sitosterol alleviates atherosclerosis by regulating catalase, Heliyon. 10 (2024) e35639. https://doi.org/https://doi.org/10.1016/j.heliyon.2024.e35639.

[66] T. Yokota, K. Nomura, M. Nagashima, et al., Fucoidan alleviates high-fat diet-induced dyslipidemia and atherosclerosis in ApoE(shl) mice deficient in apolipoprotein E expression, J Nutr Biochem. 32 (2016) 46-54. https://doi.org/10.1016/j.jnutbio.2016.01.011.

[67] W. Li, W. Zhi, J. Zhao, et al., Cinnamaldehyde attenuates atherosclerosis via targeting the IκB/NF-κB signaling pathway in high fat diet-induced ApoE(-/-) mice, Food Funct. 10 (2019) 4001-4009. https://doi.org/10.1039/c9fo00396g.

[68] M. Xiong, C. Jia, J. Cui, et al., Shexiang Tongxin dropping pill attenuates atherosclerotic lesions in ApoE deficient mouse model, J Ethnopharmacol. 159 (2015) 84-92. https://doi.org/10.1016/j.jep.2014.11.013.

[69] Y. Wu, F. Wang, L. Fan, et al., Baicalin alleviates atherosclerosis by relieving oxidative stress and inflammatory responses via inactivating the NF-κB and p38 MAPK signaling pathways, Biomed Pharmacother. 97 (2018) 1673-1679. https://doi.org/10.1016/j.biopha.2017.12.024.

[70] X. Fu, S. Zhai, J. Yuan, Endothelial HuR deletion reduces the expression of proatherogenic molecules and attenuates atherosclerosis, Int Immunopharmacol. 65 (2018) 248-255. https://doi.org/10.1016/j.intimp.2018.09.023.

[71] P. Libby, J. Loscalzo, P.M. Ridker, et al., Inflammation, Immunity, and Infection in Atherothrombosis: JACC Review Topic of the Week, J Am Coll Cardiol. 72 (2018) 2071-2081. https://doi.org/10.1016/j.jacc.2018.08.1043.

[72] S.A. Jang, D.W. Park, J.E. Kwon, et al., Quinic acid inhibits vascular inflammation in TNF-α-stimulated vascular smooth muscle cells, Biomed Pharmacother. 96 (2017) 563-571. https://doi.org/10.1016/j.biopha.2017.10.021.

[73] A.A. Mangoni, A. Zinellu, S. Sotgia, et al., Protective Effects of Methotrexate against Proatherosclerotic Cytokines: A Review of the Evidence, Mediators Inflamm. 2017 (2017) 9632846. https://doi.org/10.1155/2017/9632846.

[74] I. Csige, D. Ujvárosy, Z. Szabó, et al., The Impact of Obesity on the Cardiovascular System, J Diabetes Res. 2018 (2018) 3407306. https://doi.org/10.1155/2018/3407306.

[75] P. Sucharda, [Obesity and atherosclerosis--what's the link?], Vnitr Lek. 56 (2010) 289-291.

[76] H. Raeisi-Dehkordi, M. Amiri, K.H. Humphries, et al., The Effect of Canola Oil on Body Weight and Composition: A Systematic Review and Meta-Analysis of Randomized Controlled Clinical Trials, Adv Nutr. 10 (2019) 419-432. https://doi.org/10.1093/advances/nmy108.

[77] Y. Lu, Y. Chen, R. Li, et al., Protective effects of Danzhi jiangtang capsule on vascular endothelial damages induced by high-fat diet and palmitic acid, Biomed Pharmacother. 107 (2018) 1631-1640. https://doi.org/10.1016/j.biopha.2018.08.129.

[78] G. Chen, H. Li, Y. Zhao, et al., Saponins from stems and leaves of Panax ginseng prevent obesity via regulating thermogenesis, lipogenesis and lipolysis in high-fat diet-induced obese C57BL/6 mice, Food Chem Toxicol. 106 (2017) 393-403. https://doi.org/10.1016/j.fct.2017.06.012.

[79] L. Qu, Q. Liu, Q. Zhang, et al., Kiwifruit seed oil prevents obesity by regulating inflammation, thermogenesis, and gut microbiota in high-fat diet-induced obese C57BL/6 mice, Food Chem Toxicol. 125 (2019) 85-94. https://doi.org/10.1016/j.fct.2018.12.046.

[80] S. Zhang, F. Hong, C. Ma, et al., Hepatic Lipid Metabolism Disorder and Atherosclerosis, Endocr Metab Immune Disord Drug Targets. 22 (2022) 590-600. https://doi.org/10.2174/1871530322666211220110810.

[81] Y. Lu, Q. Wu, L.Z. Liu, et al., Pyridostigmine protects against cardiomyopathy associated with adipose tissue browning and improvement of vagal activity in high-fat diet rats, Biochim Biophys Acta Mol Basis Dis. 1864 (2018) 1037-1050. https://doi.org/10.1016/j.bbadis.2018.01.006.

[82] R. Ren, J. Gong, Y. Zhao, et al., Sulfated polysaccharide from Enteromorpha prolifera suppresses SREBP-1c and ACC expression to lower serum triglycerides in high-fat diet-induced hyperlipidaemic rats, J. Funct. Foods. 40 (2018) 722-728. https://doi.org/https://doi.org/10.1016/j.jff.2017.12.010.

[83] H. Liu, X. Qi, K. Yu, et al., AMPK activation is involved in hypoglycemic and hypolipidemic activities of mogroside-rich extract from Siraitia grosvenorii (Swingle) fruits on high-fat diet/streptozotocin-induced diabetic mice, Food Funct. 10 (2019) 151-162. https://doi.org/10.1039/c8fo01486h.

[84] H. Tilg, T.E. Adolph, M. Trauner, Gut-liver axis: Pathophysiological concepts and clinical implications, Cell Metab. 34 (2022) 1700-1718. https://doi.org/10.1016/j.cmet.2022.09.017.

[85] J.Y.L. Chiang, J.M. Ferrell, Y. Wu, et al., Bile Acid and Cholesterol Metabolism in Atherosclerotic Cardiovascular Disease and Therapy, Cardiol Plus. 5 (2020) 159-170.

[86] F.R. Ponziani, A. Nesci, C. Caputo, et al., High prevalence of lower limb atherosclerosis is linked with the gut-liver axis in patients with primary biliary cholangitis, Liver Int. 43 (2023) 370-380. https://doi.org/10.1111/liv.15463.

[87] F. Wang, C. Zhao, G. Tian, et al., Naringin Alleviates Atherosclerosis in ApoE(-/-) Mice by Regulating Cholesterol Metabolism Involved in Gut Microbiota Remodeling, J Agric Food Chem. 68 (2020) 12651-12660. https://doi.org/10.1021/acs.jafc.0c05800.

[88] K. Kasahara, R.L. Kerby, Q. Zhang, et al., Gut bacterial metabolism contributes to host global purine homeostasis, Cell Host & Microbe. 31 (2023) 1038-1053.e1010. https://doi.org/https://doi.org/10.1016/j.chom.2023.05.011.

[89] A. Giedraitiene, V. Tatarunas, K. Kaminskaite, et al., Enterobacterales Biofilm-Specific Genes and Antimicrobial and Anti-Inflammatory Biomarkers in the Blood of Patients with Ischemic Heart Disease, Diagnostics (Basel). 14 (2024) https://doi.org/10.3390/diagnostics14050546.

[90] T. Wu, Q. Yu, Y. Luo, et al., Whole-Grain Highland Barley Attenuates Atherosclerosis Associated with NLRP3 Inflammasome Pathway and Gut Microbiota in ApoE(-/-) Mice, Nutrients. 15 (2023) https://doi.org/10.3390/nu15194186.

[91] J. Mo, J. Ni, M. Zhang, et al., Mulberry Anthocyanins Ameliorate DSS-Induced Ulcerative Colitis by Improving Intestinal Barrier Function and Modulating Gut Microbiota, Antioxidants (Basel). 11 (2022) https://doi.org/10.3390/antiox11091674.

[92] D. Dong, T. Su, W. Chen, et al., Clostridioides difficile aggravates dextran sulfate solution (DSS)-induced colitis by shaping the gut microbiota and promoting neutrophil recruitment, Gut Microbes. 15 (2023) 2192478. https://doi.org/10.1080/19490976.2023.2192478.

[93] J. Cheng, D. Liu, Y. Huang, et al., Phlorizin Mitigates Dextran Sulfate Sodium-Induced Colitis in Mice by Modulating Gut Microbiota and Inhibiting Ferroptosis, J Agric Food Chem. 71 (2023) 16043-16056. https://doi.org/10.1021/acs.jafc.3c01497.